Depositional age models in lacustrine systems from zircon and carbonate U-Pb geochronology

Damaris Montano, Marta Gasparrini, Sébastien Rohais, Richard Albert, Axel Gerdes

▶ **To cite this version:**

Damaris Montano, Marta Gasparrini, Sébastien Rohais, Richard Albert, Axel Gerdes. Depositional age models in lacustrine systems from zircon and carbonate U-Pb geochronology. Sedimentology, 2022, 69 (6), pp.2507-2534. 10.1111/sed.13000 . hal-03943796

HAL Id: hal-03943796
https://ifp.hal.science/hal-03943796

Submitted on 17 Jan 2023

HAL is a multi-disciplinary open access archive for the deposit and dissemination of scientific research documents, whether they are published or not. The documents may come from teaching and research institutions in France or abroad, or from public or private research centers.

L'archive ouverte pluridisciplinaire **HAL**, est destinée au dépôt et à la diffusion de documents scientifiques de niveau recherche, publiés ou non, émanant des établissements d'enseignement et de recherche français ou étrangers, des laboratoires publics ou privés.

Distributed under a Creative Commons Attribution - NonCommercial - NoDerivatives 4.0 International License

SEDIMENTOLOGY
the journal of the International Association of Sedimentologists

Sedimentology (2022) **69**, 2507–2534 doi: 10.1111/sed.13000

Depositional age models in lacustrine systems from zircon and carbonate U-Pb geochronology

DAMARIS MONTANO*,†,‡,§, MARTA GASPARRINI¶, SÉBASTIEN ROHAIS*, RICHARD ALBERT†,‡ and AXEL GERDES†,‡
**IFP Energies nouvelles, 1 et 4 avenue de Bois-Préau, 92852, Rueil-Malmaison, France*
†Institut für Geowissenschaften, Goethe University Frankfurt, Altenhöferallee 1, 60438 Frankfurt am Main, Germany
‡Frankfurt Isotope and Element Research Center (FIERCE), Goethe-Universität Frankfurt am Main, Altenhöferallee 1, 60438, Frankfurt am Main, Germany
§Sorbonne Université, ED 398 – GRNE, 4, place Jussieu, 75252, Paris, France
¶Department of Earth Sciences "Ardito Desio", Università degli Studi di Milano, via L. Mangiagalli 34, Milan, 20133, Italy (E-mail: marta.gasparrini@unimi.it)

Associate Editor – Mike Rogerson

ABSTRACT

The Yacoraite Formation (Salta rift, Argentina) consists of Maastrichtian–Danian lacustrine carbonate and siliciclastic deposits with interbedded volcanic ash layers, organized in four third-order stratigraphic sequences. It offers the exceptional opportunity to jointly apply *in situ* zircon and carbonate U-Pb geochronology that resulted in two distinct depositional age depth models. Ages of the youngest zircon population from ash layers were linearly interpolated to derive a zircon depositional age depth model. A carbonate depositional age depth model was instead obtained from dated carbonate phases including microbialites, ooids, oncoids of calcitic and dolomitic mineralogy as well as early lacustrine calcite cements. Mean ages were defined from different carbonate phases belonging to the same layer and then linearly interpolated. Sedimentation rates were calculated from both depth models between pairs of dated samples and used to estimate the age of sequence boundaries, as well as the duration of the four stratigraphic sequences. The zircon and carbonate depositional age depth models agree with biostratigraphic constraints and exhibit excellent consistency. The onset and end of sedimentation were estimated at 68.2 ± 0.9 Ma and 62.3 ± 0.6 Ma (duration *ca* 5.7 Ma) via zircon geochronology and at 67.9 ± 1.7 Ma and 61.9 ± 1.3 Ma (duration *ca* 6.0 Ma) via carbonate geochronology. Results from this study show that with suitable samples and a newly implemented working strategy, *in situ* U-Pb dating of depositional and early diagenetic carbonates represent a valuable chronostratigraphic tool for estimating sedimentation rate and duration in poorly time-framed depositional systems.

Keywords Depositional age model, lacustrine deposits, Maastrichtian–Danian, sedimentation rate, U-Pb geochronology, Yacoraite Formation.

© 2022 The Authors. *Sedimentology* published by John Wiley & Sons Ltd on behalf of International Association of Sedimentologists

This is an open access article under the terms of the Creative Commons Attribution-NonCommercial-NoDerivs License, which permits use and distribution in any medium, provided the original work is properly cited, the use is non-commercial and no modifications or adaptations are made.

13653091, 2022, 6, Downloaded from https://onlinelibrary.wiley.com/doi/10.1111/sed.13000 by Ifp Energies Nouvelles, Wiley Online Library on [17/01/2023]. See the Terms and Conditions (https://onlinelibrary.wiley.com/terms-and-conditions) on Wiley Online Library for rules of use; OA articles are governed by the applicable Creative Commons License

INTRODUCTION

Lacustrine carbonate and siliciclastic deposits represent high resolution sedimentary archives recording environmental, tectonic and climate forcing (e.g. Kelts & Talbot, 1990; Leng & Marshall, 2004). Lacustrine deposits are also increasingly investigated by the oil and gas industry since they host major hydrocarbon accumulations (e.g. Bohacs *et al.*, 2000; Katz, 2001; Thompson *et al.*, 2015; Ceraldi & Green, 2016; Saller *et al.*, 2016). The reconstruction of the depositional history as well as the estimation of sedimentation rates in these settings are usually hampered by the scarcity of index taxa and by the problematic recovery of short duration palynomorph biozones (e.g. Wainman *et al.*, 2018). Sedimentation rates in particular represent key modulators of proxies used to reconstruct the depositional system palaeoenvironmental conditions (Crombez *et al.*, 2020), and are fundamental parameters for backstripping analysis and subsidence curve restoration (Berra & Carminati, 2010). Their estimation is even more challenging in lacustrine basins where they may vary by several orders of magnitude due to the influence of climate, tectonic and depositional processes (e.g. Enos, 1991; Einsele, 2001).

Uranium–lead geochronology has proven to be a useful tool to assess for zircon depositional ages (ZDA) and for the temporal evolution of sedimentation rates of continental sedimentary successions deposited coevally with volcanic events. Hence, the age of the youngest concordant zircon population is considered as the best approximation of the host rock depositional age (e.g. Lehrmann *et al.*, 2006; Wotzlaw *et al.*, 2014; Schoene *et al.*, 2015; Rossignol *et al.*, 2019). However, absolute radiometric constraints are often absent in most continental settings. Therefore, in such settings, a complex multiproxy analysis based on sedimentology, stratigraphy, magnetostratigraphy and diagenesis is usually needed to reconstruct the depositional history and the sedimentation rate evolution over time (Schumer & Jerolmack, 2009; Cartier *et al.*, 2018; Frisch *et al.*, 2019).

Radiometric age determination of carbonates has been a long-standing problem in geochronology. Since the pioneering work of Smith & Farquhar (1989) it has been recognized that U-Pb carbonate geochronology has the potential to directly provide the timing of carbonate precipitation, although this was initially limited by the low success rate, moderate precision and time-consuming dating procedures (Rasbury & Cole, 2009). The advent of the LA-ICP-MS (laser ablation–inductively coupled plasma–mass spectrometry) U-Pb geochronology of carbonates (LAcarb) increased the success rate of carbonate dating by ensuring a higher spatial resolution (Rasbury *et al.*, 2021). However, LAcarb is currently applied mainly to calcite cements to date fluid flow events (e.g. Mangenot *et al.*, 2018; Walter *et al.*, 2018; Cruset *et al.*, 2020; Mottram *et al.*, 2020; Roberts *et al.*, 2020a,b, 2021; Bilau *et al.*, 2021; Yang *et al.*, 2022). Recent advances on sample selection and screening techniques (e.g. Drost *et al.*, 2018; Guillong *et al.*, 2020; Roberts *et al.*, 2020a; Rasbury *et al.*, 2021) have greatly improved the ability to target depositional and early diagenetic carbonates, and to calculate ages with adequate precision for chronostratigraphic and palaeoenvironmental studies (e.g. Brigaud *et al.*, 2021; Montano *et al.*, 2021). It is noteworthy that, in contrast to zircon geochronology, ages obtained from depositional and early diagenetic carbonates (carbonate depositional ages; CDA) should be considered as minimum time constraints for deposition. This is because carbonates are highly susceptible to diagenetic processes (for example, stabilization, recrystallization and replacement) that may affect the U-Pb systematic and consequently degrade or reset the original ages (Jones *et al.*, 1995; Kelly *et al.*, 2003; Li *et al.*, 2014; Roberts *et al.*, 2020a). In spite of this, LAcarb dating may provide ages consistent, within uncertainties, with biostratigraphic and radiometric constraints. This has been shown for meteoric cements in speleothems (Hopley *et al.*, 2019; Woodhead & Petrus, 2019; Nicholson *et al.*, 2020) and hardgrounds (Liivamägi *et al.*, 2018; Scardia *et al.*, 2019; Kurumada *et al.*, 2020; Brigaud *et al.*, 2021; Środoń *et al.*, 2022), lacustrine tufa, micrites and associated cements (Drost *et al.*, 2018; Frisch *et al.*, 2019; Parrish *et al.*, 2019; Hoareau *et al.*, 2021; Montano *et al.*, 2021; Rasbury *et al.*, 2021), marine cements (Meinhold *et al.*, 2020; Hoareau *et al.*, 2021) and bioclasts (Drost *et al.*, 2018). Despite these remarkable results, no study has attempted to define, solely based on LAcarb, a robust depositional age depth model along an entire stratigraphic section, which was also dated by zircon geochronology. The Yacoraite Formation (Maastrichtian–Danian, north-west Argentina) represents an ideal target for such purpose. It consists of lacustrine carbonate and siliciclastic deposits interbedded with volcanic ash layers and organized in four third-order stratigraphic sequences (0.5 to 5.0 Ma; *sensu* Van Wagoner *et al.*, 1988). The structural framework,

© 2022 The Authors. *Sedimentology* published by John Wiley & Sons Ltd on behalf of International Association of Sedimentologists, *Sedimentology*, **69**, 2507–2534

13653091, 2022, 6, Downloaded from https://onlinelibrary.wiley.com/doi/10.1111/sed.13000 by ifp Energies Nouvelles, Wiley Online Library on [17/01/2023]. See the Terms and Conditions (https://onlinelibrary.wiley.com/terms-and-conditions) on Wiley Online Library for rules of use; OA articles are governed by the applicable Creative Commons License

stratigraphic architecture and diagenetic history of this formation are well-known from literature (Hernandez *et al.*, 1999; Cesaretti *et al.*, 2000; Sial *et al.*, 2001; Durieux & Brown, 2007; Marquillas *et al.*, 2007; Rohais *et al.*, 2019; Deschamps *et al.*, 2020; Gomes *et al.*, 2020). In this study, volcanic ash layers were sampled together with carbonates along a stratigraphic section and investigated for petrography and U-Pb analysis. Concordia ages were obtained from ash layer zircon grains whereas weighted average ages were computed from depositional and early diagenetic carbonates coexisting in the same layer.

Concordia ages from zircon and weighted average ages from carbonates were linearly interpolated to build ZDA and CDA depth models. The sedimentation rates, calculated from these models, were used to constrain the ages of sequence boundaries as well as the duration of third-order stratigraphic sequences.

The present study provides insights on the carbonate dating potential together with a newly implemented working strategy to reconstruct depositional age depth models in various sedimentary settings. It reveals that models based on LAcarb may have the potential to assist chronostratigraphy studies in systems with poor time constraints.

GEOLOGICAL SETTING AND GEOCHRONOLOGICAL BACKGROUND

The Salta rift basin in north-west Argentina (Fig. 1) belongs to the Andean Cretaceous–Palaeogene basin system of central-western South America. Structural highs separate the southern branch of the Salta rift basin into three main sub-basins: the El Rey, Alemania and Metán sub-basins (Salfity & Marquillas, 1994). The main tectonic stages of rift evolution are recorded by the Pirgua (syn-rift deposits; Reyes & Salfity, 1973), the Balbuena (transitional sag deposits) and the Santa Barbara (post-rift deposits) groups (Moreno, 1970). The Balbuena Group includes, from base to top, the Lecho, the Yacoraite and the Tunal/Olmedo formations. The Lecho Formation mainly consists of aeolian to fluvio-lacustrine sandstones whereas the Tunal/Olmedo formations are made of playa lake deposits, including evaporites along with some fine-grained clastics (Salfity, 1979).

The Yacoraite Formation was deposited in lacustrine to shallow marine environments coevally with the main stage of rift thermal subsidence and tectonic quiescence (Salfity & Marquillas, 1994; Starck, 2011). It dominantly consists of shales, mudstones, oolitic packstones to grainstones and microbial boundstones, interbedded with fine-grained to coarse-grained sandstones (e.g. Salfity, 1979; Marquillas, 1985; Salfity & Marquillas, 1994; Hernandez *et al.*, 1999; Deschamps *et al.*, 2020; Gomes *et al.*, 2020). Volcanic ashes occur interbedded with the sedimentary succession (e.g. Marquillas *et al.*, 2011; Rohais *et al.*, 2019). They are known to be coeval with the Palmar Largo volcanism (70 to 60 Ma; Fernandez, 1975; Mädel, 1984; Gómez-Omil *et al.*, 1987; Omarini *et al.*, 1989; Disalvo *et al.*, 2002), although they were also attributed to the Late Cretaceous volcanic arc of northern Chile (Marquillas *et al.*, 2011) and have provided one of the oldest, recycled zircon grains of South America (3.7 Ga; Paquette *et al.*, 2015).

The stratigraphic architecture of the Yacoraite Formation has been studied since the 1980s (e.g. Marquillas, 1985; Salfity & Marquillas, 1994; Hernandez *et al.*, 1999). The present contribution takes into account recent studies that have established a robust basin-scale stratigraphic framework (Rohais *et al.*, 2019; Deschamps *et al.*, 2020). Accordingly, the Yacoraite Formation is subdivided into four third-order sequences (mid-term sequences of *ca* 1 Ma duration; Deschamps *et al.*, 2020), organized in a second order sequence (long-term sequence of *ca* 5 Ma; Deschamps *et al.*, 2020). The four third-order sequences are bounded by five sequence boundaries (SB) usually associated with a major backstepping of the depositional system and erosion in proximal domains. According to biostratigraphic constraints, the age of the Yacoraite Formation is Maastrichtian–Danian. Indeed, the Lecho and Yacoraite formations host well-preserved Senonian dinosaur bones and tracks (Raskovsky, 1968; Reyes, 1972; Alonso & Marquillas, 1986; Marquillas *et al.*, 2003; Cónsole-Gonella *et al.*, 2017) and palynological associations of Maastrichtian age (Moroni, 1982; Quattrocchio *et al.*, 2005; Quattrocchio, 2006), whereas the Tunal/Olmedo formations are characterized by Danian palynological associations (Volkheimer *et al.*, 2006). A 12 Ma depositional time duration (75 to 63 Ma) was proposed for the Yacoraite Formation by correlating the sediment regressive/transgressive cycles with the global sea-level curve (Hernandez *et al.*, 1999). Such an approach is hampered by the limited connection of the Salta basin with the ocean and by the fact that the lake level dynamics and the global sea-

© 2022 The Authors. *Sedimentology* published by John Wiley & Sons Ltd on behalf of International Association of Sedimentologists, *Sedimentology*, **69**, 2507–2534

13653091, 2022, 6, Downloaded from https://onlinelibrary.wiley.com/doi/10.1111/sed.13000 by ifp Energies Nouvelles, Wiley Online Library on [17/01/2023]. See the Terms and Conditions (https://onlinelibrary.wiley.com/terms-and-conditions) on Wiley Online Library for rules of use; OA articles are governed by the applicable Creative Commons License

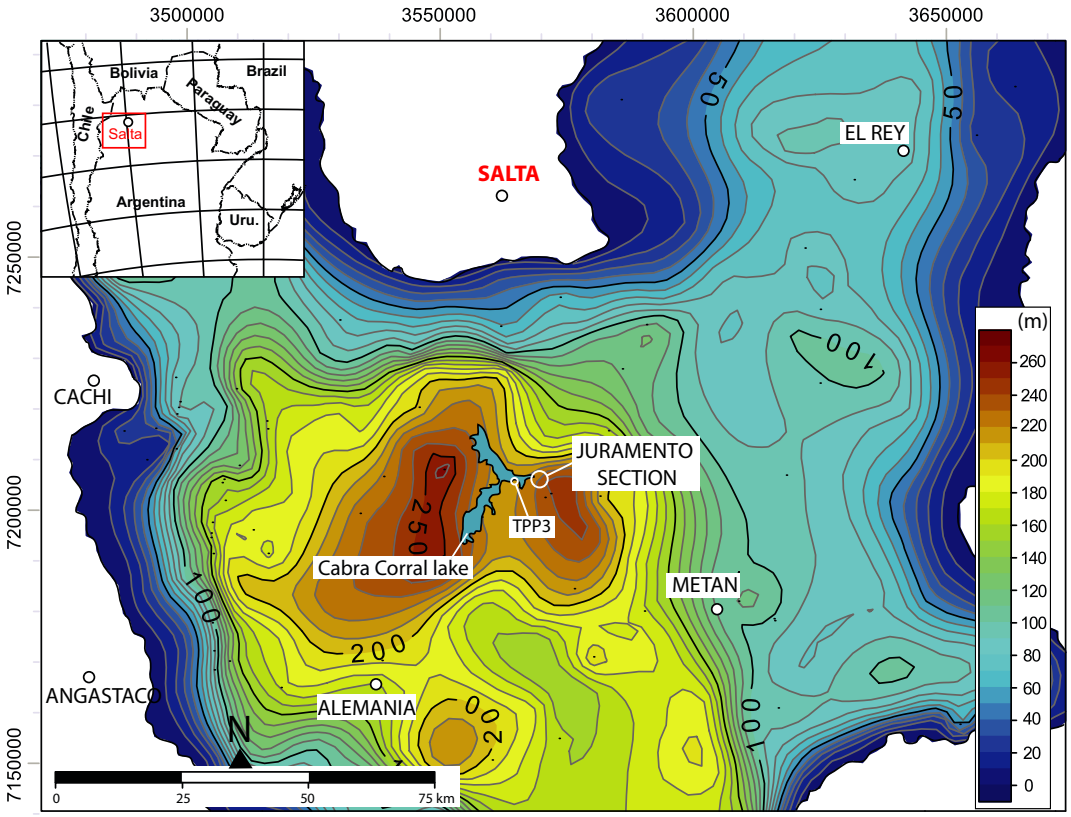

Fig. 1. (A) Location of the Salta rift basin in north-west Argentina. (B) Present day thickness map of the Yacoraite Formation in the Metán and Alemania sub-basins with the position of Juramento stratigraphic section and TPP3 ash sample. Modified from Rohais *et al.* (2019).

level curve are out of phase by different orders of magnitude (e.g. Gebhardt *et al.*, 2017). Zircon U-Pb geochronology of the Yacoraite Formation ash layers provided absolute ages spanning from 71.9 ± 0.4 Ma to 60.3 ± 2.1 Ma (Marquillas *et al.*, 2011; Pimentel *et al.*, 2012; Rohais *et al.*, 2019), though inconsistencies among the different datasets exist and are discussed in section *ZDA depth model via zircon geochronology*.

MATERIALS AND METHODS

Investigated samples

Carbonates and volcanic ashes were sampled from the Yacoraite Formation along a stratigraphic section named Juramento (25°18′08.01″S, 65°17′42.91″W) from the Cabra Corral lake area of the Metán sub-basin (Fig. 1). This section, located close to one of the main depocentres, was chosen to minimize the occurrence of major hiatuses that characterize the proximal domains (Deschamps *et al.*, 2020). The sedimentology and stratigraphy of the Juramento section, as well as the position of all carbonate and ash layer samples are detailed in Fig. 2. Twelve carbonate samples (JUR1, JUB1, JUB5, JUB6, CH1, JUB7, JUR8, JUR25, JURC6, JURC10, JURD3 and JURD9) were collected, together with five volcanic ash samples (TJ0, TJ3, TJ4, TJ7 and TJ8) interbedded with the sedimentary succession. One additional ash sample (TPP3) was collected from sequence 4 of a stratigraphic section located *ca* 4 km away (25°17′27″S, 65°21′15″W; Fig. 1). According to the stratigraphic correlations proposed by Rohais *et al.* (2019) and Deschamps *et al.* (2020) the TPP3 sample was projected to *ca* 219 m from the base of the Juramento section, where a thin ash layer also occurs.

Macroscopic and microscopic analysis of ash layers and carbonates

Ash layers were chosen in the field based on features such as thickness, absence of re-sedimentation/reworking evidence and naked-eye

© 2022 The Authors. *Sedimentology* published by John Wiley & Sons Ltd on behalf of International Association of Sedimentologists, *Sedimentology*, **69**, 2507–2534

13653091, 2022, 6, Downloaded from https://onlinelibrary.wiley.com/doi/10.1111/sed.13000 by Ifp Energies Nouvelles, Wiley Online Library on [17/01/2023]. See the Terms and Conditions (https://onlinelibrary.wiley.com/terms-and-conditions) on Wiley Online Library for rules of use; OA articles are governed by the applicable Creative Commons License

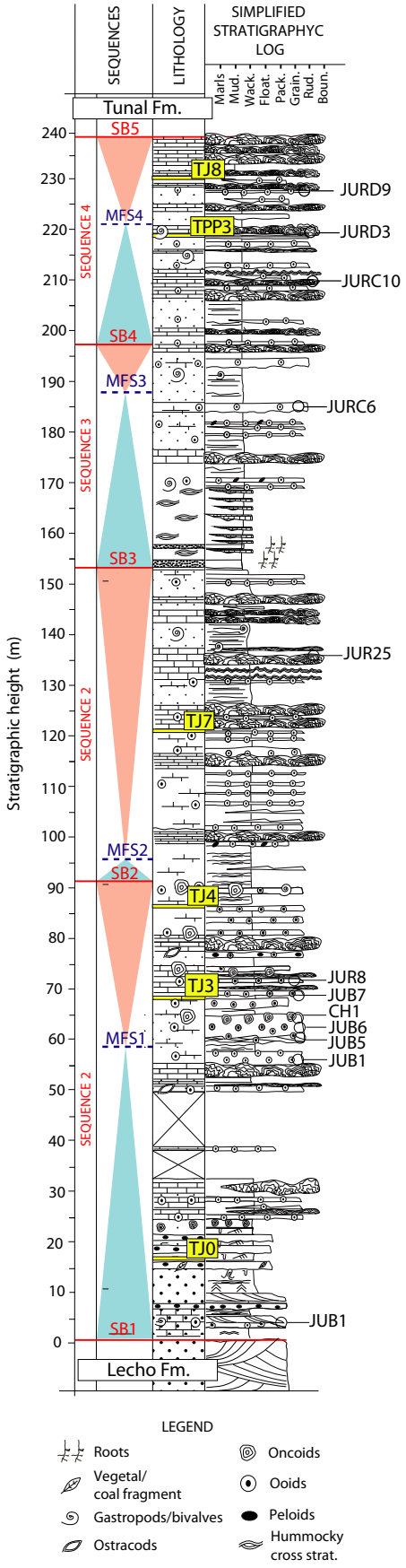

Fig. 2. Sedimentological column and sequence stratigraphy of the Yacoraite Formation from the Juramento section. Position of the sequence boundaries (SB, in red) and maximum flooding surfaces (MFS, in blue) along the section are after Rohais *et al.* (2019) and Deschamps *et al.* (2020). The names of carbonate and ash layer samples investigated are indicated in black and yellow, respectively. Boun., boundstone; Float., floatstone; Grain., grainstone; Mud., mudstone; Pack., packstone; Rud., rudstone; Wack., wackestone.

component heterogeneity. The collected material (2 to 4 kg for each ash layer) was prepared for petrographic analysis and isotope dating in the FIERCE (Frankfurt Isotope and Element Research Center, Goethe University Frankfurt, Germany). The material was fragmented by high voltage discharge using a SelFrag Lab system (Selfrag AG, Kerzers, Switzerland) and then sieved to <280 μm using disposable nylon sieves. Dense grains were then separated through manual panning. Up to 182 zircon grains were randomly handpicked for each ash layer sample to get a representative selection of the overall zircon populations and to minimize sampling bias. The grains were embedded in epoxy resin and ground down to about half their thickness and then polished. Zircon petrography under a binocular microscope was followed by scanning electron microscope (SEM) analysis. Cathodoluminescence (CL) and back scattered electron (BSE) images were acquired using a JEOL JSM-6490 SEM (JEOL Limited, Tokyo, Japan).

Carbonate samples were selected away from mineralized fractures and exposure surfaces to avoid potential overprinting by later fluids. Carbonate textures were described by using the Dunham (1962) classification, whereas facies and depositional environments were attributed following the scheme proposed by Deschamps *et al.* (2020). In this respect, the term stromatolite may include the microbial boundstone that here will be simply named microbialite.

Twelve polished and uncovered thin sections (50 to 60 μm thick), one for each carbonate sample collected, were prepared for petrographic analysis to characterize the different facies and to identify various depositional and diagenetic carbonate phases. Additionally, petrographic studies aimed to identify carbonate phases with no evidence of post-depositional diagenetic modifications. Conventional optical petrography was performed using a Nikon ECLIPSE LV100 POL polarized light microscope (Nikon, Tokyo,

© 2022 The Authors. *Sedimentology* published by John Wiley & Sons Ltd on behalf of International Association of Sedimentologists, *Sedimentology*, **69**, 2507–2534

13653091, 2022, 6, Downloaded from https://onlinelibrary.wiley.com/doi/10.1111/sed.13000 by Ifp Energies Nouvelles, Wiley Online Library on [17/01/2023]. See the Terms and Conditions (https://onlinelibrary.wiley.com/terms-and-conditions) on Wiley Online Library for rules of use; OA articles are governed by the applicable Creative Commons License

Japan) and allowed observations under plane-polarized and cross-polarized light (PPL and XPL). Cathodoluminescence (CL) optical microscopy was accomplished with a cold CL instrument (8200 Mk5; Cambridge Image Technology Limited, Cambridge, UK) whose electron beam worked under vacuum (<0.1 mbar) with an acceleration voltage of 10 kV and a current of 250 μA. All thin sections were partially stained with a solution of 10% diluted HCl, Alizarin red-S and potassium ferricyanide (Dickson, 1966). Calcite cement habitus were described based on the Flügel (2004) classification scheme.

Zircon U-Pb geochronology

Zircon grains from the six ash layers sampled were analyzed for U, Th and Pb isotopes by LA-ICP-MS at FIERCE, following the methods described by Gerdes & Zeh (2006, 2009). A Thermo Scientific Element XR sector field ICP-MS (Thermo Fisher Scientific, Waltham, MA, USA) was coupled to a RESOlution 193 nm ArF Excimer laser (CompexPro 102; Coherent Inc, Santa Clara, CA, USA) equipped with an S-155 two-volume ablation cell (Laurin Technic Pty, Canberra, ACT, Australia). The data were acquired in four analytical sessions in 2018 to 2019. The settings of the laser and the ICP-MS instruments are given in Appendix S1. The GJ-1 zircon (Jackson *et al.*, 2004) was used as primary zircon reference material (RM) and BB-16 (Santos *et al.*, 2017), 91500 (Wiedenbeck *et al.*, 1995), Plešovice (Sláma *et al.*, 2008) and Monastery (Kamenetsky *et al.*, 2014) zircon RMs for validation of the analytical results. The results obtained on these RMs were within 0.8% or better of the reported ages. Data processing (including common Pb correction) was performed using an Isoplot (Ludwig, 2012) supported Microsoft Excel®-based spreadsheet (Gerdes & Zeh, 2006, 2009). Uncertainties are reported at the 2σ level and are calculated by quadratic addition of the internal uncertainties (SE), counting statistics, background uncertainties, common Pb corrections, excess of scatter (derived from the primary RM) and the excess of variance calculated from the offset (or calibrator) RM. A second uncertainty is reported and expands the previous one with systematic uncertainties. These are the long-term variance (0.8%, 2σ) and the decay constant uncertainties (see Horstwood *et al.*, 2016). Concordia diagrams (2σ precision ellipses) and Concordia ages were calculated using Isoplot 4.15 (Ludwig, 2012) and associated $MSWD_{C+E}$ (i.e. mean squared weighted deviation of concordance and equivalence).

Carbonate U-Pb geochronology

Twelve thin sections were analyzed in one U-Pb LA-ICP-MS analytical session at FIERCE using the same instrumentation as for the zircon grains. Prior to analysis, thin sections were cleaned in an ultrasonic bath with ethanol. During the LA-session the ablation parameters were kept constant for all samples and reference materials. The unstained portions of the thin sections were ablated in a helium atmosphere (300 ml min^{-1}) and mixed in the ablation funnel with argon (1 L min^{-1}) and nitrogen (6 to 8 ml min^{-1}). Analyses were performed with square ablation spots (213 μm × 213 μm), 8 Hz repetition rate and a fluence of about 2 J cm^{-2}. A manual pre-screening session allowed identifying areas with high and variable U/Pb and $^{207}Pb/^{206}Pb$ ratios. The settings of the laser and the ICPMS instrument are given in Appendix S1.

Raw data were corrected off-line using the same Isoplot (Ludwig, 2012) supported Microsoft Excel®-based spreadsheet (Gerdes & Zeh, 2006, 2009) as for the zircon analyses. Fractionation of $^{238}U/^{206}Pb$, $^{207}Pb/^{206}Pb$ ratios and their drift were corrected based on repeated analyses of soda-lime glass NIST-SRM 614. WC-1 calcite RM (Roberts *et al.*, 2017) was used to correct for the matrix offset (5%) between NIST glass and carbonate. Results were plotted in U-Pb Tera-Wasserburg Concordia plots using Isoplot 4.15 (Ludwig, 2012) and ages were calculated as the intersection of the regression lines with the Concordia curve. Regression lines were constrained with 13 to 40 ablation spots (N) for each of the investigated carbonate phases. All uncertainties are reported at 2σ and were calculated as described in the zircon dating methodology. Speleothem calcite ASH-15D (Nuriel *et al.*, 2021) was measured as the validation RM. No common Pb corrections were applied and the long-term variance used is 1.5% (2σ; Montano *et al.*, 2021).

RESULTS

Ash layer and zircon description

The sampled volcanic ash deposits (TJ0, TJ3, TJ4, TJ7, TJ8 and TPP3) consist of consolidated

© 2022 The Authors. *Sedimentology* published by John Wiley & Sons Ltd on behalf of International Association of Sedimentologists, *Sedimentology*, **69**, 2507–2534

13653091, 2022, 6, Downloaded from https://onlinelibrary.wiley.com/doi/10.1111/sed.13000 by Ifp Energies Nouvelles, Wiley Online Library on [17/01/2023]. See the Terms and Conditions (https://onlinelibrary.wiley.com/terms-and-conditions) on Wiley Online Library for rules of use; OA articles are governed by the applicable Creative Commons License

centimetre-thick to decimetre-thick tabular to lenticular layers characterized by a white to yellowish colour easily recognizable in fresh outcrops (Fig. 3). Grain mineralogy is heterogeneous, so that ash layers consist of variable amounts of quartz, feldspar, plagioclase, biotite, hornblende, monazite, muscovite, garnet, apatite, zircon and other unidentified opaque minerals. Zircon grains are 50 to 150 μm long and appear mostly clear and colourless and only rarely yellowish or pinkish. They commonly exhibit euhedral long-prismatic to needle-like shape. Some grains show signs of resorption and rounded edges. Scanning electron microscope images show the presence of well-preserved oscillatory zoning in most of the grains. Many of them display a central tube or a channel filled with glassy material (i.e. frozen melt), which together with the CL zonation indicates a volcanic origin (Pupin, 1976).

Carbonate facies and petrography

The carbonate samples analyzed include five different sedimentary facies: fine-grained stromatolite (JUR25, JURC10 and JURD3 samples; Fig. 4A and B), sandy oolitic grainstone (JUR1 sample), grapestone–ooid grainstone to packstone (JURD9 sample; Fig. 4C), oolitic grainstone (JUB1, JUB7, JUR8 and JURC6 samples; Fig. 4D to F) and oncoidal rudstone (JUB5, JUB6 and CH1 samples; Fig. 4G and H). Petrographic analysis allowed identification of different depositional carbonate phases characterized by calcitic, dolomitic or mixed (i.e. calcite and dolomite) mineralogy. The phases analyzed are: calcitic ooids (OC), mixed ooids (OM), calcitic microbialites (MIC-C), dolomitic microbialites (MIC-D) and dolomitic oncoids (OND).

The fine-grained stromatolite samples are always characterized by the alternation of calcitic (MIC-C) and dolomitic (MIC-D) planar to convoluted microbial laminae that reach a few millimetres in thickness (Fig. 4A and B) and may build up centimetre-sized to decimetre-sized domal structures (Fig. 4A). The laminae have a heterogeneous mineralogy and may host calcite and dolomite microcrystals, together with authigenic pyrite and quartz grains (Fig. 4B). The sandy oolitic grainstone sample is poorly sorted and made of >50% rounded to subangular, mostly monocrystalline, quartz grains, 100 to 500 μm in size as well as dispersed ooids. The grapestone–ooid grainstone to packstone sample includes flat calcitic stromatolite clasts (MIC-C), calcitic ooids (OC) locally organized in lumps, and angular to subangular quartz grains, 100 to 200 μm in size (Fig. 4C). The oolitic grainstone samples (Fig. 4D to F) include calcitic ooids (OC), dolomitic ooids (OD) and mixed ooids (OM), the latter displaying an alternation of calcitic and dolomitic cortex laminae (Fig. 4E). The oncoidal rudstone samples are made of dolomitic spongiostromate oncoids (OND) with size up to 2 mm and a microporous centre (Fig. 4G and H).

Most samples are cemented by an early diagenetic calcite, named EC (Fig. 4D) and made by blocky crystals (*ca* 150 μm in size) with zoned dull orange luminescence. The EC precipitated in the interparticle and framework pores. It formed before the sediments underwent mechanical compaction as suggested by the limited grain-to-grain contacts observed in samples where this cement occurs (Fig. 4D and F). The EC is post-dated by other blocky calcite cements, named LC1 and LC2, which also fill interparticle pores and are respectively bright orange and non-luminescent (Fig. 4F and H).

Zircon and carbonate U-Pb geochronology

Zircon crystals of magmatic origin were selected for analysis based on grain shape and internal oscillatory zoning. The aim of this selection was to determine the youngest zircon crystallization event to date the deposition of the ash layer. It must be taken into account that the selected grains may also include zircon antecrysts crystallizing during an earlier pulse in the magma chamber, as well as xenocrysts that the magma assimilated from the wall rocks or during magma transport.

The 294 zircon grains analyzed yielded $^{206}Pb/^{238}U$ dates ranging between 35 Ma to 1.1 Ga, with dominant density distribution peaks around 60 to 70 Ma and around 500 Ma (Appendix S1). About half of the zircon grains (141) produced $^{206}Pb/^{238}U$ dates <100 Ma. Among them, 119 fall in a tight cluster at 63 to 68 Ma on the Concordia curve (i.e. concordant zircon dates) and 14 do not overlap with their error ellipses on the Concordia curve (i.e. discordant zircon dates). The remaining eight analyses have apparently concordant $^{206}Pb/^{238}U$ dates and form, together with five of the discordant analyses, a cluster between 60 to 35 Ma. These grains were found only in samples TJ4 and TPP3 (Appendix S1). It is worth noting that no grains yielded concordant ages between 71 Ma

© 2022 The Authors. *Sedimentology* published by John Wiley & Sons Ltd on behalf of International Association of Sedimentologists, *Sedimentology*, **69**, 2507–2534

13653091, 2022, 6, Downloaded from https://onlinelibrary.wiley.com/doi/10.1111/sed.13000 by Ifp Energies Nouvelles, Wiley Online Library on [17/01/2023]. See the Terms and Conditions (https://onlinelibrary.wiley.com/terms-and-conditions) on Wiley Online Library for rules of use; OA articles are governed by the applicable Creative Commons License

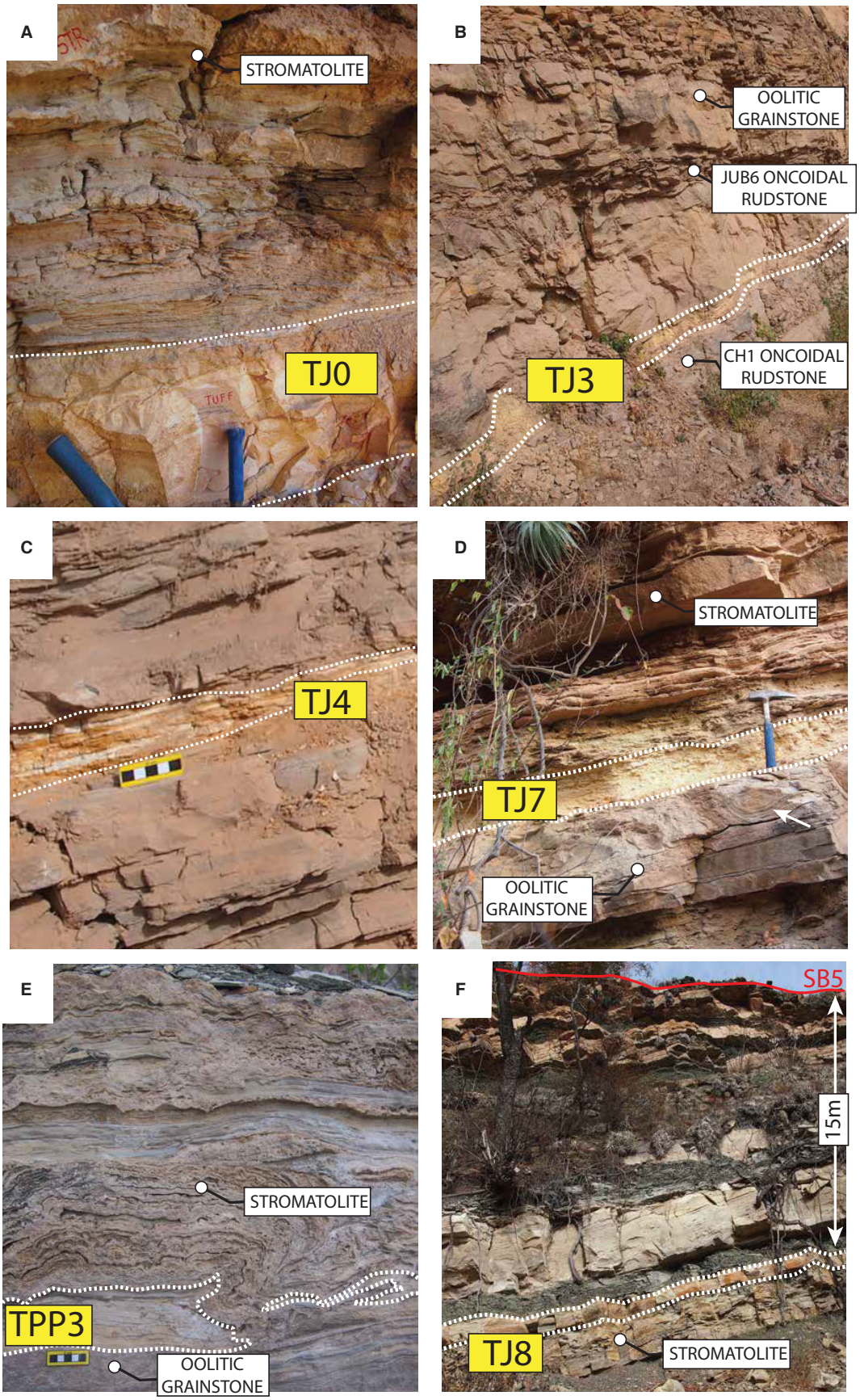

© 2022 The Authors. *Sedimentology* published by John Wiley & Sons Ltd on behalf of International Association of Sedimentologists, *Sedimentology*, **69**, 2507–2534

13653091, 2022, 6, Downloaded from https://onlinelibrary.wiley.com/doi/10.1111/sed.13000 by Ifp Energies Nouvelles, Wiley Online Library on [17/01/2023]. See the Terms and Conditions (https://onlinelibrary.wiley.com/terms-and-conditions) on Wiley Online Library for rules of use; OA articles are governed by the applicable Creative Commons License

Fig. 3. Field photographs and location of the sampled volcanic ash layers, occurring interbedded within the sedimentary deposits in the Yacoraite Formation. Ash layers are highlighted by dashed white lines. (A) Light yellow to light pink 30 cm thick massive tabular volcanic ash layer overlaid by laminated siltstone to sandstone with current ripples. The decimetre-size rounded domes at the top represents the first stromatolite occurring along the Juramento section. TJ0 ash layer, sequence 1, clastic shoreface facies association, 15 m from the base. Photograph width corresponds to approximately 1.5 m. GPS coordinates: 25°18′06.12″S – 65°18′52.7″W. (B) Light yellow, *ca* 30 cm thick lenticular ash layer in a carbonate dominated outcrop. TJ3 ash layer, sequence 1, ooid banks facies association, 68 m from the base. Photo width corresponds to approximately 3 m. GPS coordinates: 25°18′05.7″S – 65°17′49.1″W. (C) White to light yellow lenticular ash layer, 5 to 10 cm thick, showing internal lamination. TJ4 ash layer, sequence 1, eulittoral facies association, 87 m from the base. Photograph width corresponds to approximately 70 cm. GPS coordinates: 25°18′05.7″S – 65°17′47.8″W. (D) Tabular 20 cm thick ash layer overlying oolitic grainstone with fluid expulsion features (see white arrow). TJ7 ash layer, sequence 2, high-energy eulittoral facies association, 121 m from the base. The hammer for scale is 35 cm long. GPS coordinates: 25°18′08″S – 65°17′47.8″W. (E) Moustache-like thinly laminated stromatolite growing into a lenticular yellowish ash layer. TPP3 ash layer, sequence 4, alternating marginal lacustrine facies association, 219 m from the base. The yellow scale is 5 cm. GPS coordinates: 25°17′01.5″S – 65°21′34.6″W. (F) Tabular, decimetre-thick ash layer interbedded within greenish marl and massive carbonate deposits. TJ8 ash layer, sequence 4, alternating marginal lacustrine facies association, 232 m from the base. GPS coordinates: 25°18′13.8″S – 65°17′36.3″W.

and 90 Ma. The Th/U ratios of the 63 to 68 Ma cluster range from 0.36 to 2.5, being consistent with a magmatic origin (Williams & Claesson, 1987).

Zircon grains from the 63 to 68 Ma cluster were detected in all samples except in TJ8. They form statistically meaningful and equivalent populations of concordant ages associated with $MSWD_{C+E} \leq 2$ (Table 1; Fig. 5). In TJ0 sample the young zircon population is poorly represented, with nine of the 71 zircon grains yielding a Concordia age of 67.55 ± 0.60/0.89 Ma ($MSWD_{C+E}$ of 1.3). The remaining 62 analyzed grains were all xenocrysts clustering on Concordia around 430 to 570 Ma and 1.0 to 1.1 Ga. In the TJ3 ash layer, 29 out of the 55 analyzed grains form an equivalent age group, with a Concordia age of 67.87 ± 0.33/0.64 Ma ($MSWD_{C+E}$ of 1.5). In addition, four grains with a Concordia age of 70.69 ± 0.72/0.91 Ma ($MSWD_{C+E}$ of 0.88) constitute another independent population, probably associated with an earlier magma pulse. In the TJ4 ash layer, 27 zircon grains were analyzed and, among them, 20 grains define a homogeneous group with a Concordia age of 66.27 ± 0.27/0.59 Ma ($MSWD_{C+E}$ = 1.4). The remaining discordant to apparently concordant analyses produced $^{206}Pb/^{238}U$ dates ranging from 63 to 45 Ma. In TJ7 sample, 11 equivalent dates were detected over 55 zircon grains. They yielded a Concordia age of 65.35 ± 0.56/0.77 Ma ($MSWD_{C+E}$ = 2.0). The remaining 55 grains are xenocrysts, as shown by their $^{206}Pb/^{238}U$ dates ranging from 150 Ma to 1.1 Ga. All zircon grains selected in TPP3 ash layer sample yielded $^{206}Pb/^{238}U$ dates <65 Ma. Forty-five grains defined an equivalent group, with a Concordia age of 63.33 ± 0.26/0.56 Ma ($MSWD_{C+E}$ = 1.3). The remaining nine grains gave apparently concordant ages that range from 55 to 43 Ma. Sample TJ8 was characterized by poor zircon yield and by the occurrence of xenocrysts only. Eight out of 21 grains provided $^{206}Pb/^{238}U$ dates plotting on the Concordia between 420 Ma and 720 Ma. From the 12 carbonate samples studied, a total of 22 carbonate phases were analyzed: calcitic, dolomitic and mixed ooids (n = 6), calcitic and dolomitic microbialites (n = 7), dolomitic oncoids (n = 3) and EC cement (n = 6). U and Pb concentrations were very variable, ranging from 0.23 to 7.30 ppm and from 0.02 to 12.55 ppm, respectively. The $^{238}U/^{206}Pb$ and $^{207}Pb/^{206}Pb$ isotope ratios of all analyzed carbonate phases vary from 0.25 to 89.06 and from 0.09 and 0.84, respectively. The highest $^{238}U/^{206}Pb$ and $^{207}Pb/^{206}Pb$ isotope ratio variability corresponds to the EC cement, whereas all the other phases display $^{238}U/^{206}Pb$ isotope ratios mostly below 30 (see Appendix S1).

Some of the Tera–Wasserburg Concordia diagrams with lower intercept ages are displayed in Fig. 6, while the complete dataset is reported in Appendix S2. Three of the 22 carbonate phases analyzed (calcitic ooids from samples JURD9 and JURC10 and calcitic microbialite from sample JURD9) could not be dated because of too homogeneous or too scattered U-Pb isotope ratios (see Appendix S1). The remaining 19 carbonate phases (86% of the total) yielded well-defined regression lines with lower intercept ages between 67.32 ± 1.92 Ma and 58.88 ± 2.58 Ma and MSWD (i.e. mean squared

© 2022 The Authors. *Sedimentology* published by John Wiley & Sons Ltd on behalf of International Association of Sedimentologists, *Sedimentology*, **69**, 2507–2534

13653091, 2022, 6, Downloaded from https://onlinelibrary.wiley.com/doi/10.1111/sed.13000 by Ifp Energies Nouvelles, Wiley Online Library on [17/01/2023]. See the Terms and Conditions (https://onlinelibrary.wiley.com/terms-and-conditions) on Wiley Online Library for rules of use; OA articles are governed by the applicable Creative Commons License

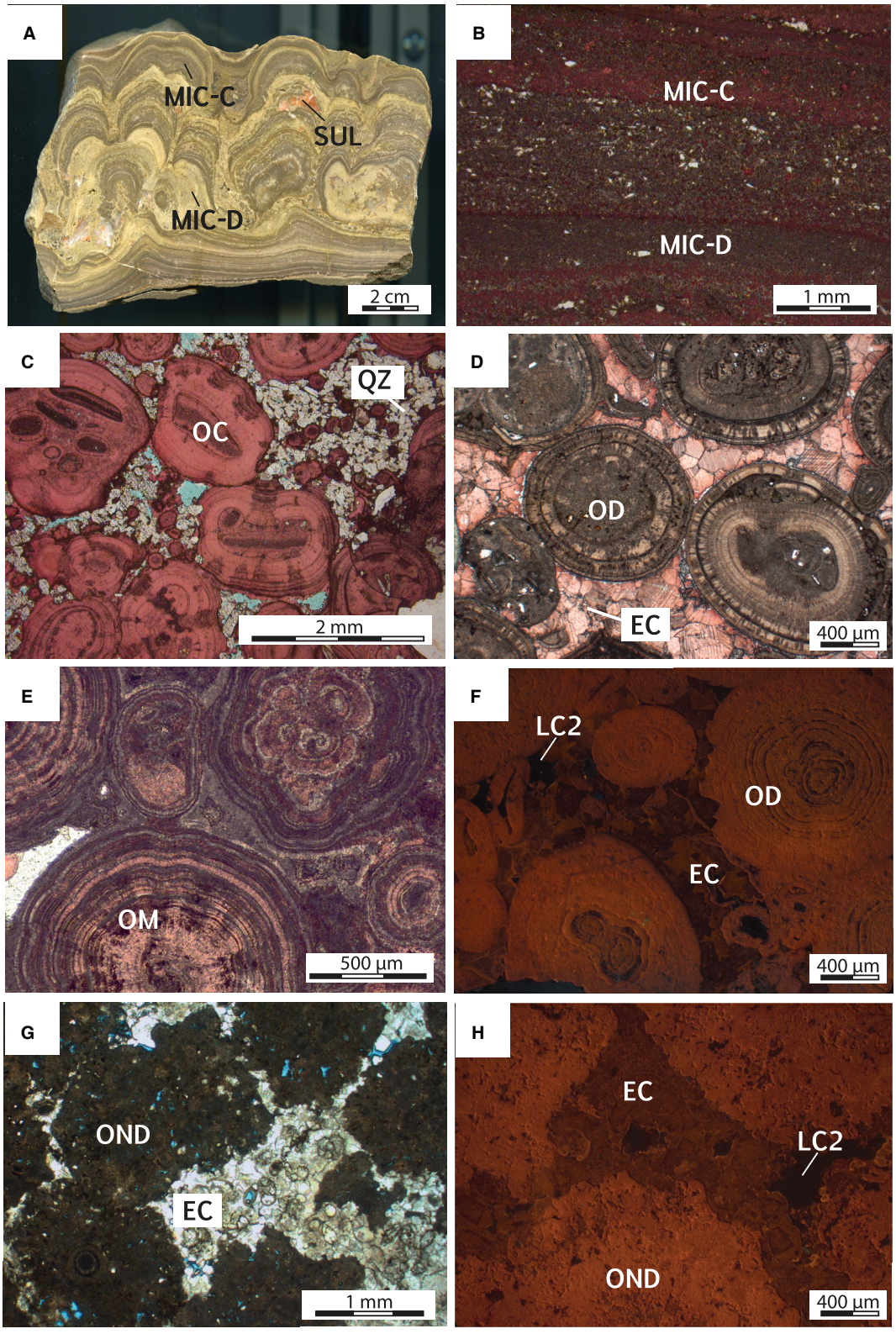

weighted deviates) from 0.5 to 1.8. The precision obtained (expressed as 2σ) ranges from 1.4 to 6.3% (2σ, Table 1), with just one age (i.e. dolomitic microbialite from the JURC10 sample) displaying an internal uncertainty of 16.7% (2σ).

© 2022 The Authors. *Sedimentology* published by John Wiley & Sons Ltd on behalf of International Association of Sedimentologists, *Sedimentology*, **69**, 2507–2534

13653091, 2022, 6, Downloaded from https://onlinelibrary.wiley.com/doi/10.1111/sed.13000 by Ifp Energies Nouvelles, Wiley Online Library on [17/01/2023]. See the Terms and Conditions (https://onlinelibrary.wiley.com/terms-and-conditions) on Wiley Online Library for rules of use; OA articles are governed by the applicable Creative Commons License

Fig. 4. Mesoscopic and petrographic images of the carbonate samples investigated. (A) Laminated to columnar fine-grained stromatolite displaying an alternation of calcitic (grey) and dolomitic (beige) sub-millimetric laminae, indicated respectively with MIC-C and MIC-D – see (B). Authigenic minerals such as sulphates (SUL) also occur. JUR25, rock-slab scan. (B) Fine-grained laminated stromatolite characterized by the alternation of pink stained (non-ferroan) calcitic laminae (MIC-C) and unstained (non-ferroan) dolomitic laminae (MIC-D). JURD3 sample, stained, PPL view. (C) Grapestone–ooid grainstone to packstone composed by non-ferroan calcitic ooids (OC) and quartz grains (QZ). JURD9 sample, stained, PPL view. (D) Oolitic grainstone made of non-ferroan dolomitic ooids (OD), cemented by a non-ferroan blocky calcite (EC). JUR8 sample, stained, PPL view. (E) Oolitic grainstone given by mixed ooids (OM) displaying an alternation of calcitic and dolomitic cortex laminae (OM). JUB1 sample, stained, PPL view. (F) Oolitic grainstone made of dolomitic ooids (OD) cemented by early blocky calcite (EC) with a zoned dull orange luminescence, followed by non-luminescent calcite (LC2). JUB7 sample, stained, CL view. (G) Oncoidal rudstone composed by porous dolomitic spongiostromate oncoids (OND) cemented by early blocky calcite (EC). JUB5 sample, PPL view. (H) Oncoidal rudstone with dolomitic spongiostromate oncoids (OND) cemented by early blocky calcite (EC) with dull orange zoned luminescence, followed by non-luminescent calcite (LC2). JUB5 sample, CL view.

DISCUSSION

ZDA depth model via zircon geochronology

To define a robust ZDA depth model for the Yacoraite Formation, six volcanic ash layers (TJ0, TJ3, TJ4, TJ7, TPP3 and TJ8) cropping out in the Metán sub-basin (Figs 1 and 2) were examined and mostly showed no reworking features (Fig. 3). Except for the TJ8 ash layer, all the samples included a group of equivalent and concordant zircon ages between 63 Ma and 68 Ma (Fig. 6). Unlike the high precision ID-TIMS (isotope dilution – thermal ionization mass spectrometry) methods (e.g. Wotzlaw *et al.*, 2014), the LA-ICP-MS technique employed can resolve relative differences in zircon age populations down to ±0.6% (2σ; around ±0.4 Ma for 66 Ma deposits). However, the precision achieved proved suitable for the present study. The ZDA obtained agree with the Maastrichtian–Danian biostratigraphic constraints (e.g. Moroni, 1982, 1984; Volkheimer *et al.*, 2006; Valais & Cónsole-Gonella, 2019) and clearly gets younger up-section, with the exception of TJ4 sample (66.27 ± 0.27/0.59 Ma) which appears to be slightly older than TJ3 sample (65.87 ± 0.33/0.64 Ma), although within uncertainty limits (Figs 5 and 7).

The ZDA obtained in this study and by previous authors (Marquillas *et al.*, 2011; Pimentel *et al.*, 2012; Rohais *et al.*, 2019) were taken into account (Table 2; Fig. 7) to build the ZDA depth model along the Juramento stratigraphic section. To do so, dated ash layers that do not crop out along the Juramento section were projected onto it according to the stratigraphic correlations of Rohais *et al.* (2019) and Deschamps *et al.* (2020). It is worth mentioning that Marquillas *et al.* (2011), Pimentel *et al.* (2012) and Rohais *et al.* (2019) provided partially contradictory results (Fig. 7), and that only Rohais *et al.* (2019) followed the uncertainty propagation procedure recommended by Horstwood *et al.* (2016). In contrast to the previous authors, the ZDA ages here calculated take into account the expanded uncertainties, which include the long-term external reproducibility of the method (0.8%; 2σ).

The ZDA from the present study agree within uncertainties with the ages reported by Rohais *et al.* (2019) but not with those from Marquillas *et al.* (2011) and Pimentel *et al.* (2012) (Fig. 7). Marquillas *et al.* (2011) dated zircon grains from two volcanic ash layers, one located at 56 m and the other projected at 186.4 m from the base of the section, obtaining ages of 71.9 ± 0.4 Ma and 68.4 ± 0.7 Ma, respectively (Table 2; Fig. 7). These ages are about 3 to 4 Ma older than those obtained by Rohais *et al.* (2019) via replicate analyses on the same ash layers. Pimentel *et al.* (2012) dated two layers, the Basal tuff (63.4 ± 0.9 Ma) and the Top tuff (60.3 ± 2.1 Ma), which are projected on the Juramento section at 185 m and 230 m, respectively (Fig. 7). The Basal tuff has been dated in multiple analytical sessions by Rohais *et al.* (2019) and yielded younger and consistent ZDA of 65.1 ± 0.5 Ma (see TUF3 in Table 2) and 64.8 ± 0.5 (see TUFF PP05 in Table 2). The Top tuff age, the youngest ever proposed for the top of the Yacoraite Formation, led workers to conclude that sedimentation ended at around 60 Ma (Bento-Freire, 2012; Sial *et al.*, 2013; Gomes *et al.*, 2020). However, the low accuracy (3.5%, 2σ; Table 2) and the high MSWD (6.9;

© 2022 The Authors. *Sedimentology* published by John Wiley & Sons Ltd on behalf of International Association of Sedimentologists, *Sedimentology*, **69**, 2507–2534

13653091, 2022, 6, Downloaded from https://onlinelibrary.wiley.com/doi/10.1111/sed.13000 by Ifp Energies Nouvelles, Wiley Online Library on [17/01/2023]. See the Terms and Conditions (https://onlinelibrary.wiley.com/terms-and-conditions) on Wiley Online Library for rules of use; OA articles are governed by the applicable Creative Commons License

Table 1. U-Pb geochronology data obtained for the zircon and carbonate samples investigated. Carbonate phases are: calcitic microbialite (MIC-C), dolomitic microbialite (MIC-D), dolomitic ooids (OD), mixed ooids (OM), dolomitic oncoids (OND) and early blocky calcite cement (EC).

Strat. height (m)	Sequence	Sample	Phase	Age* (Ma)	$2\sigma_i$ † (Ma)	$2\sigma_i$ ‡ (%)	$2\sigma_{ex}$ § (Ma)	$^{207}Pb/^{206}Pb \pm 2\sigma$ ¶	*n***	MSWD††
232	4	TJ8	Zircon	–	–	–	–	–	–	–
219		TPP3	Zircon	63.33	0.26	0.41	0.56	–	45	1.30
217		JURD3	MIC-C	63.44	1.53	2.41	1.80	0.8204 ± 0.0015	40	1.79
		JURD3	MIC-D	62.58	2.05	3.28	2.26	0.8244 ± 0.0029	18	0.82
211		JURC10	MIC-C	63.66	1.44	2.26	1.73	0.8254 ± 0.0045	19	0.82
		JURC10	MIC-D	66.81	11.15	16.69	11.20	0.8260 ± 0.0067	13	0.61
185	3	JURC6	OM	64.25	2.48	3.86	2.66	0.8230 ± 0.0040	24	0.74
		JURC6	EC	64.51	1.73	2.68	1.98	0.8105 ± 0.0014	16	1.01
136	2	JUR25	MIC-C	64.31	2.64	4.11	2.81	0.8258 ± 0.0032	29	0.67
		JUR25	MIC-D	63.62	3.98	6.26	4.09	0.8337 ± 0.0053	22	1.58
121		TJ7	Zircon	65.35	0.56	0.86	0.77	–	11	2.0
87	1	TJ4	Zircon	66.27	0.27	0.40	0.59	–	20	1.40
71		JUR8	OD	65.11	3.27	5.02	3.41	0.8212 ± 0.0019	20	0.97
		JUR8	EC	66.45	1.22	1.84	1.58	0.8131 ± 0.0105	15	1.62
68		JUB7	OD	65.52	2.06	3.14	2.29	0.8222 ± 0.0015	25	0.59
		JUB7	EC	67.32	1.63	2.42	1.92	0.8282 ± 0.0023	21	1.25
67.5		TJ3	Zircon	65.87	0.33	0.50	0.64	–	29	1.50
66		CH1	OND	65.49	1.47	2.24	1.77	0.8204 ± 0.0021	27	1.02
		CH1	EC	61.90	2.14	3.46	2.33	0.8156 ± 0.0027	14	1.92
65		JUB6	OND	58.88	2.43	4.13	2.58	0.8176 ± 0.0019	33	1.16
		JUB6	EC	64.73	0.96	1.48	1.37	0.8303 ± 0.0032	27	1.41
64		JUB5	OND	65.42	2.60	3.97	2.78	0.8181 ± 0.0033	20	0.50
		JUB5	EC	65.99	0.94	1.42	1.37	0.8171 ± 0.0043	15	0.98
56		JUB1	OM	65.08	3.66	5.62	3.79	0.8194 ± 0.0049	29	1.59
25.5		TJ0	Zircon	67.55	0.60	0.89	0.80	–	9	1.30

* Carbonate Tera-Wasserburg plot U-Pb lower intercept ages; zircon Concordia ages.
† Absolute internal uncertainty (without including long-term excess of variance).
‡ Relative error: percent of internal uncertainty without including long-term excess of variance.
§ Absolute uncertainty including long-term excess of variance (0.8% for ash layers, 1.5% for carbonates).
¶ Carbonate isochron y-axis intercept and absolute uncertainty = initial $^{207}Pb/^{206}Pb$ ratio.
** Number of LA-ICPMS analyses.
†† For carbonate ages is Mean Squared Weighted Deviates; for zircon ages is Mean Squared Weighted Deviates of concordance and equivalence ($MSWD_{C+E}$).

Table 2), together with the inconsistency with biostratigraphic constraints (e.g. Moroni, 1982, 1984; Volkheimer *et al.*, 2006; Valais & Cónsole-Gonella, 2019) may indicate poor reliability. Rohais *et al.* (2019) provided the most comprehensive dataset, with robust ZDA from eight ash layers cropping out in different sub-basins of the Salta rift (TUF1/1bis, TUFBBB, TUF3, PP05, CIN 8 and Ni 9; Table 2). Reworking features were reported only for the TUF2 ash layer whose U-Pb age (61.9 ± 0.7 Ma) is possibly much older than the true depositional age. In addition, the ages from Rohais *et al.* (2019) show good agreement with biostratigraphy (e.g. Moroni, 1982, 1984; Volkheimer *et al.*, 2006; Valais & Cónsole-Gonella, 2019).

In light of these findings, the ages from Marquillas *et al.* (2011), Pimentel *et al.* (2012) and the TUF2 sample of Rohais *et al.* (2019) were not considered for the computation of the ZDA depth model. Moreover, to limit the possible bias due to long distance stratigraphic correlations, only robust ages from the ash layers cropping out in the Cabra Corral lake area

13653091, 2022, 6, Downloaded from https://onlinelibrary.wiley.com/doi/10.1111/sed.13000 by Ifp Energies Nouvelles, Wiley Online Library on [17/01/2023]. See the Terms and Conditions (https://onlinelibrary.wiley.com/terms-and-conditions) on Wiley Online Library for rules of use; OA articles are governed by the applicable Creative Commons License

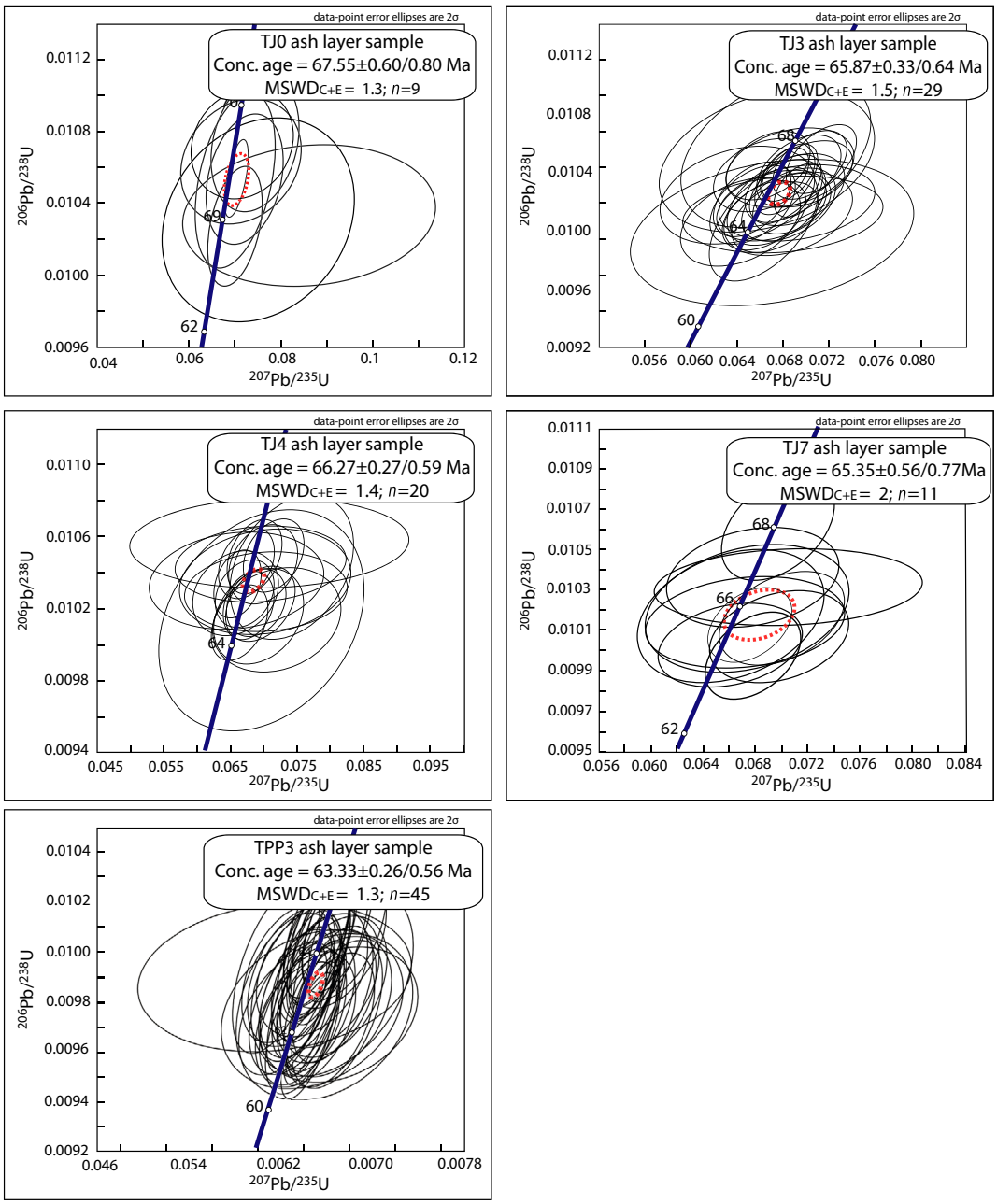

Fig. 5. $^{206}Pb/^{238}U$ versus $^{207}Pb/^{235}U$ Weatherill Concordia diagrams showing U-Pb analytical data of the zircon grains analyzed from five ash layer samples. Data point error ellipses indicate 2σ uncertainty (95% confidence). Blue line is the Concordia curve. Red dashed ellipses indicate the derived Concordia age and relative 2σ uncertainty. Concordia age results are reported with internal uncertainty (first number) and with long term excess of variance (second number). Rejected analyses are not shown (see Appendix S1).

were used (Table 2). These are TJ0, TJ3, TJ4, TJ7 and TPP3 from this study and TUF1/1bis, TUFBBB, TUF3 and PP05 from Rohais *et al.* (2019).

Various approaches may be employed to interpolate linear and non-linear age datasets along a stratigraphic section in order to build a depositional age depth model (e.g. Blaauw, 2010; Blaauw *et al.*, 2012, 2018; Lougheed & Obrochta, 2019). The Juramento stratigraphic section is located close to a basin depocentre (Fig. 1) where hiatuses >0.1 to 0.4 Ma are not expected to occur (Deschamps *et al.*, 2020) and hiatuses <0.1 to 0.4 Ma would be undetectable

© 2022 The Authors. *Sedimentology* published by John Wiley & Sons Ltd on behalf of International Association of Sedimentologists, *Sedimentology*, **69**, 2507–2534

13653091, 2022, 6, Downloaded from https://onlinelibrary.wiley.com/doi/10.1111/sed.13000 by Ifp Energies Nouvelles, Wiley Online Library on [17/01/2023]. See the Terms and Conditions (https://onlinelibrary.wiley.com/terms-and-conditions) on Wiley Online Library for rules of use; OA articles are governed by the applicable Creative Commons License

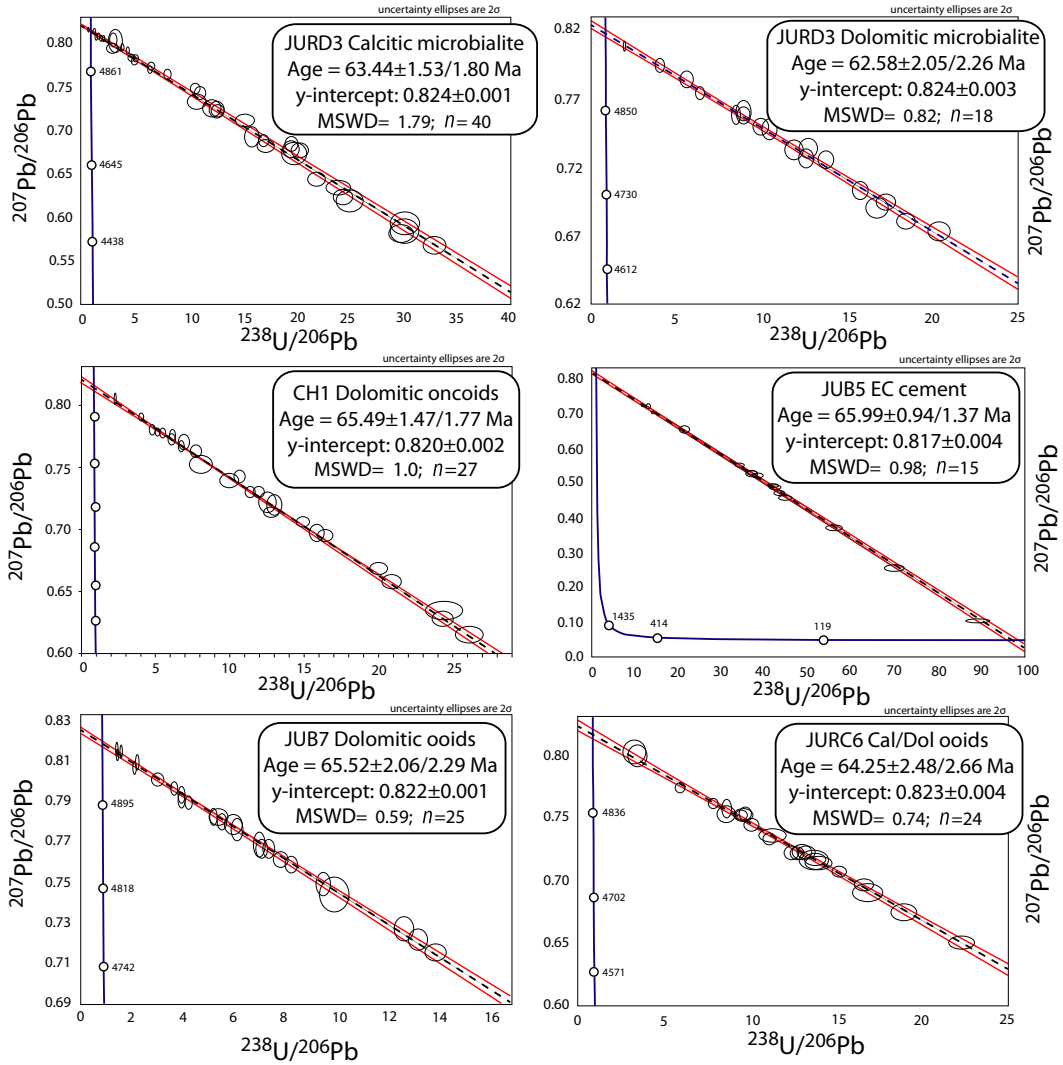

Fig. 6. $^{238}U/^{206}Pb$ versus $^{207}Pb/^{206}Pb$ Tera-Wasserburg Concordia diagrams and corresponding absolute ages for six of the carbonate samples investigated. Data point error ellipses indicate 2σ internal uncertainty (95% confidence) of the isotope ratios on '*n*' analyses. Red lines represent the envelopes of the regression lines (isochrons). In blue are the Concordia curves.

by the time resolution achieved (*ca* 0.6 Ma; 2σ). Moreover, the ages used to build the model are linearly distributed and get younger from the bottom to the top of the section (Fig. 7). For these reasons, the ZDA depth model was inferred via linear interpolation (e.g. Watson *et al.*, 2017). This is known to produce plausible age depth models that are comparable to those obtained by more advanced interpolation methods (for example, Bayesian statistics; Blaauw *et al.*, 2018). The approach used does not only provide point age depth estimates similar to the classic linear interpolation (e.g. Watson *et al.*, 2017), but also takes into account the age uncertainties. In this respect, confidence intervals for the discrete undated parts of the stratigraphic section are assigned by considering the age uncertainties of the ash layers located in close proximity. This means that in contrast to other interpolation methods (e.g. Ramsey & Lee, 2013) the uncertainties of the age model do not increase with distance from the dated layers.

The main limitation of the model produced is the absence of dated ash layers close to the bottom and top sequence boundaries of the Yacoraite Formation (i.e. SB1 and SB5). The same issue was encountered by Rohais *et al.* (2019) who estimated the age of these surfaces by calculating the

© 2022 The Authors. *Sedimentology* published by John Wiley & Sons Ltd on behalf of International Association of Sedimentologists, *Sedimentology*, **69**, 2507–2534

13653091, 2022, 6, Downloaded from https://onlinelibrary.wiley.com/doi/10.1111/sed.13000 by Ifp Energies Nouvelles, Wiley Online Library on [17/01/2023]. See the Terms and Conditions (https://onlinelibrary.wiley.com/terms-and-conditions) on Wiley Online Library for rules of use; OA articles are governed by the applicable Creative Commons License

Table 2. U-Pb geochronology data from zircon (ash layers) of the Yacoraite Formation published by previous authors.

Authors	Sample name	Location	Seq.*	Stratigraphic height (m)†	U-Pb age (Ma)	2σ‡ (Ma)	*n*§	MSWD¶
Marquillas *et al.* (2011)	AB7	Quebrada El Chorro, Río Juramento. 27.5 m above the base of the Yacoraite Formation	1	56.0	71.9	0.4	8	2.30
	TO190602	Guanaquitos section, provincial Route 47 (Cobra Corral dam), 150 m from the base of the Yacoraite Formation	1	186.4†	68.4	0.7	7	0.09
Pimentel *et al.* (2012)	Basal tuff	Assado outcrop, provincial Route 47	4	186.4†	63.4	0.9	–	–
	Upper tuff	Lomito outcrop, provincial Route 47	4	230.6†	60.3	2.1	10	6.90
Rohais *et al.* (2019)	TUF2	Juramento section	1	5.0	69.1	0.7	22	0.18
	TUF BBB	Base Bridge boat section	1	55.0†	67.0	0.7	36	0.17
	TUF1b	Juramento section	1	56.0	66.5	0.4	51	0.18
	TUF1	Juramento section	1	56.0	66.2	0.5	44	0.44
	TUF CIN8	Cachifullo section	2	90.0†	65.7	0.6	27	0.04
	Ni 9	North Isonza section	3	150.0†	65.4	1.0	9	1.60
	TUF 3	PP13 section	3	186.4†	65.1	0.9	45	0.92
	TUF PP05	PP05 section	3	186.4†	64.8	0.5	49	0.32

* Stratigraphic sequence.
† Samples from sections other than the Juramento section. Their position is projected along the Juramento section according to Rohais *et al.* (2019) and Deschamps *et al.* (2020) stratigraphic correlations.
‡ Absolute uncertainty (95% confidence) expressed in million years (Ma).
§ Number of ICP-MS spot analyses on zircons.
¶ Mean squared weighted deviates.

compacted sedimentation rates between adjacent pairs of dated layers. In this approach, sedimentation rates are assumed to remain constant during the deposition of sequences 1 and 4. The same strategy was employed here and considered TJ0 (67.55 ± 0.60/0.80 Ma) and TPP3 (63.33 ± 0.26/0.56 Ma) samples as the lowermost and uppermost ash layers dated (Fig. 7). Average sedimentation rates were calculated between pairs of dated layers by also considering the age uncertainties. These values were employed to estimate the age of sequence boundaries from which the average sedimentation rates *per* stratigraphic sequence were also calculated. Accordingly, sedimentation rates of 32 m Ma^{-1} and 20 m Ma^{-1} were computed for sequence 1 and sequence 4, respectively (Fig. 7). Based on these calculations, the sedimentation onset (SB1) and end (SB5) were estimated at 68.1 ± 0.9 Ma and 62.3 ± 0.5 Ma, respectively.

CDA depth model via carbonate geochronology

To define a CDA depth model for the Yacoraite Formation, the 19 carbonate phases dated along the Juramento section were taken into consideration (Fig. 8). Among them, 10 are dolomitic or mixed (dolomite and calcite) phases. They were also considered to infer depositional ages since dolomitization has been interpreted as syn-depositional and driven by microbial activity (Gomes *et al.*, 2020). All phases dated yielded ages from 67.30 ± 1.92 Ma to 58.88 ± 2.58 Ma ($13 < n < 40$; $2\sigma_i$ down to 1.4%; MSWD < 2; Table 1; Fig. 6, Appendix S2). Different

© 2022 The Authors. *Sedimentology* published by John Wiley & Sons Ltd on behalf of International Association of Sedimentologists, *Sedimentology*, **69**, 2507–2534

13653091, 2022, 6, Downloaded from https://onlinelibrary.wiley.com/doi/10.1111/sed.13000 by Ifp Energies Nouvelles, Wiley Online Library on [17/01/2023]. See the Terms and Conditions (https://onlinelibrary.wiley.com/terms-and-conditions) on Wiley Online Library for rules of use; OA articles are governed by the applicable Creative Commons License

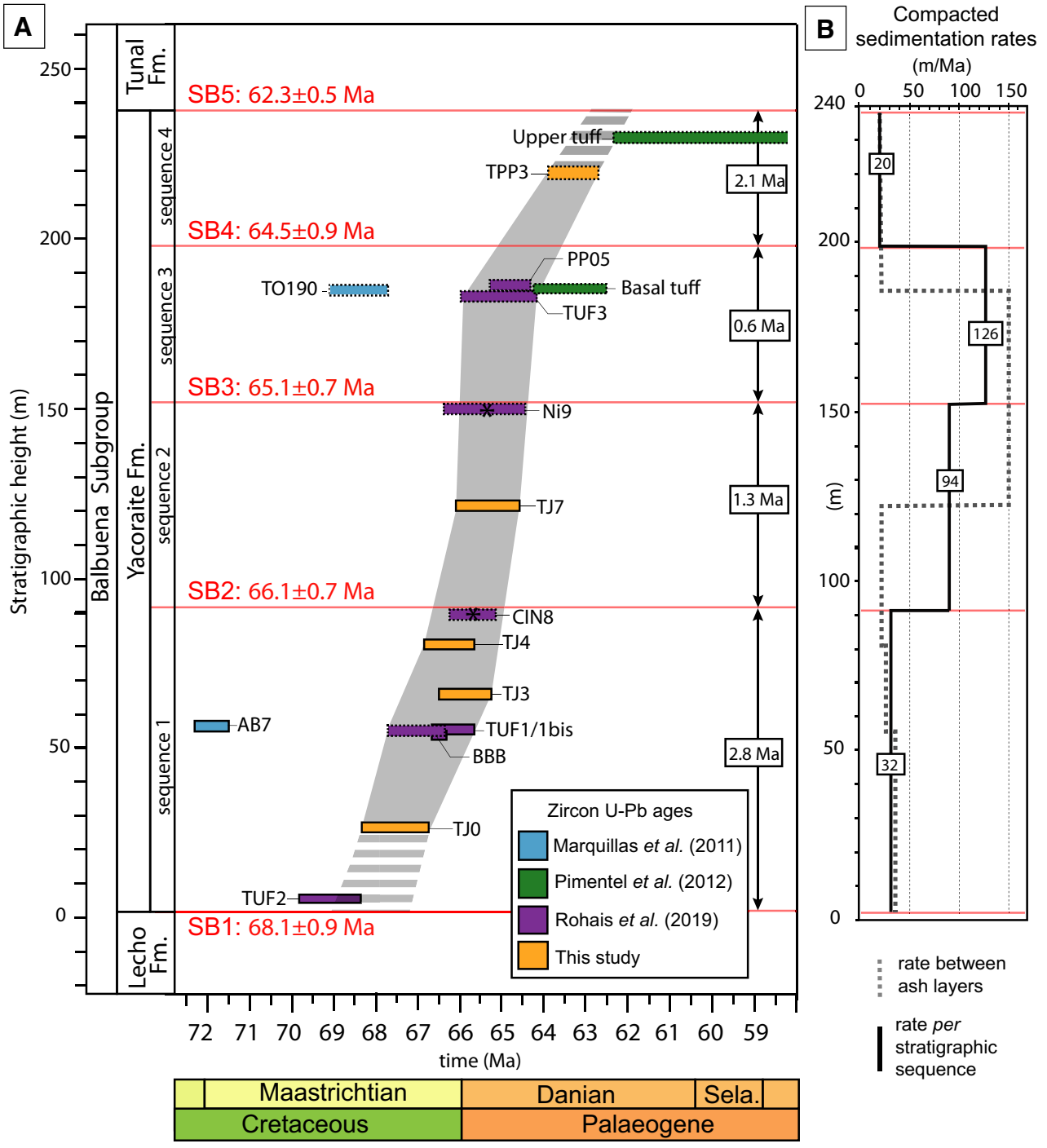

Fig. 7. Zircon depositional age (ZDA) depth model of the Yacoraite Formation from zircon (ash layer) U-Pb geochronology. Red lines are the sequence boundaries (SB). (A) Ages, uncertainties and stratigraphic positions are reported as coloured bars for all the available ash layers dated (Marquillas *et al.*, 2011; Pimentel *et al.*, 2012; Rohais *et al.*, 2019; this study). All reported uncertainties are 2σ (95% confidence). Dashed bars refer to of ash layers from the Metán and Alemania sub-basins though not along the Juramento section. Asterisks indicate ash layers from other sub-basins. The dark grey area represents the ZDA depth model obtained by linear interpolation of the zircon ages. The duration of each stratigraphic sequence is given in the black frames. (B) Evolution of the compacted sedimentation rates. The grey dashed line refers to rates calculated between dated surfaces, whereas the black line refers to weighted mean rates of each stratigraphic sequence.

© 2022 The Authors. *Sedimentology* published by John Wiley & Sons Ltd on behalf of International Association of Sedimentologists, *Sedimentology*, **69**, 2507–2534

13653091, 2022, 6, Downloaded from https://onlinelibrary.wiley.com/doi/10.1111/sed.13000 by Ifp Energies Nouvelles, Wiley Online Library on [17/01/2023]. See the Terms and Conditions (https://onlinelibrary.wiley.com/terms-and-conditions) on Wiley Online Library for rules of use; OA articles are governed by the applicable Creative Commons License

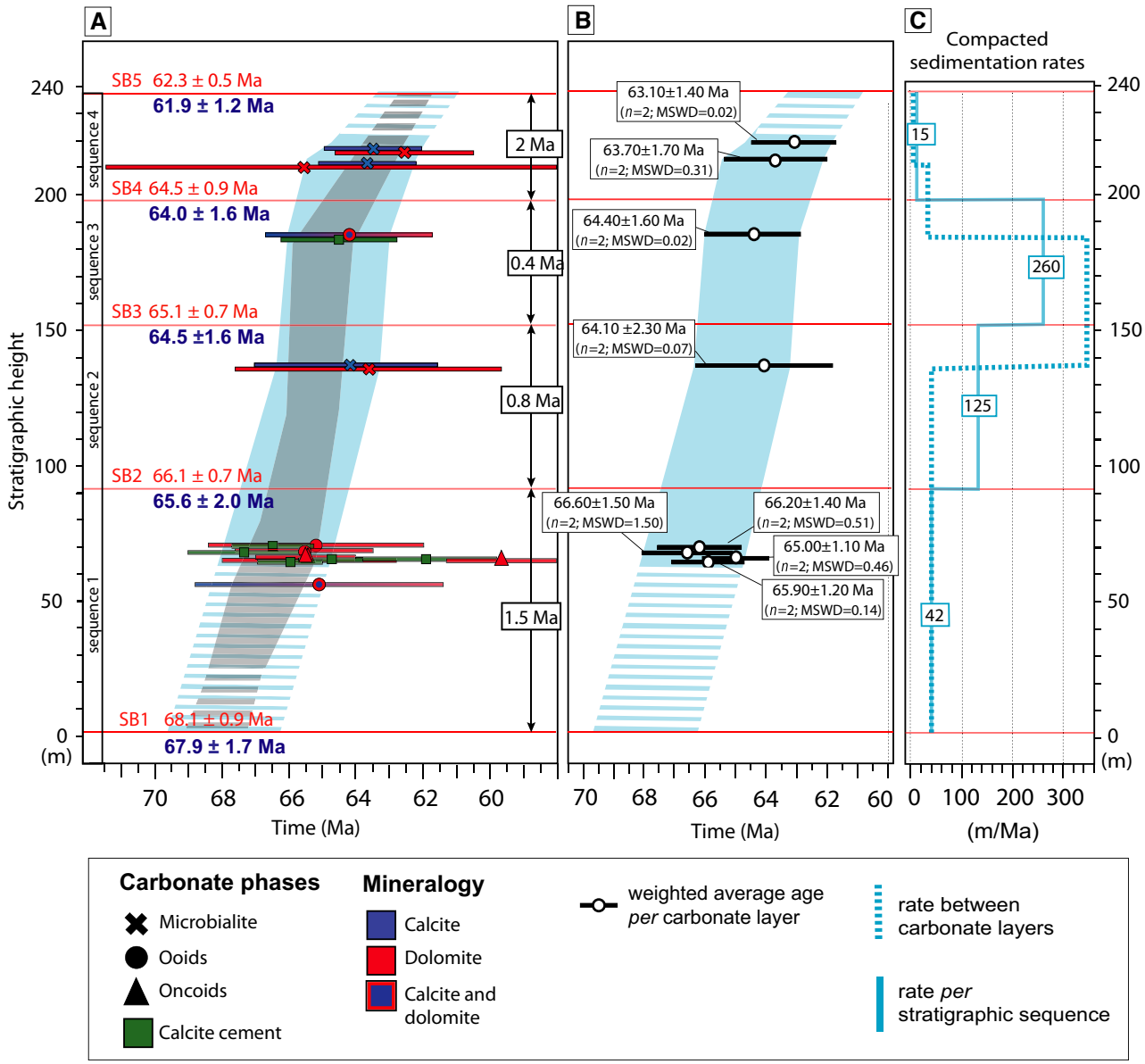

Fig. 8. Carbonate depositional age (CDA) depth model of the Yacoraite Formation from carbonate U-Pb geochronology (LAcarb). Red lines are the sequence boundaries (SB). (A) Ages, uncertainties and stratigraphic positions are reported for all carbonate phases dated in this study. The blue area represents the CDA depth model. For comparison, the ZDA depth model (light grey area) is also reported. SB ages were inferred from the ZDA (in red) and CDA (in blue) depth models. All reported uncertainties are 2σ (95% confidence). The duration of each stratigraphic sequence is given in the black frames. (B) Weighted average ages (CDAw) of carbonate phases from the same sample are reported in the black frames together with the number of single CDA considered (N) and the Mean Squared Weighted Deviates (MSWD) of the weighted average ages. The blue area represents the depth model obtained by CDAw linear interpolation. (C) Evolution of the compacted sedimentation rates along the stratigraphic section. The blue dashed line refers to rates calculated between dated carbonate samples (CDAw), whereas the blue continuous line refers to weighted mean rates for each stratigraphic sequence.

carbonate phases in the same layer mostly provided consistent results (Fig. 8A), although most dolomitic phases turned out to be associated with higher uncertainties (usually >3%, 2σ) when compared to calcitic phases (Table 1).

Two carbonate phases provided younger ages. These are the dolomitic oncoids from JUB6 sample and the blocky EC cement from CH1 sample (Table 1; Fig. 8A). The young age of the dolomitic oncoids in JUB6 sample (Fig. 9A) is

© 2022 The Authors. *Sedimentology* published by John Wiley & Sons Ltd on behalf of International Association of Sedimentologists, *Sedimentology*, **69**, 2507–2534

13653091, 2022, 6, Downloaded from https://onlinelibrary.wiley.com/doi/10.1111/sed.13000 by Ifp Energies Nouvelles, Wiley Online Library on [17/01/2023]. See the Terms and Conditions (https://onlinelibrary.wiley.com/terms-and-conditions) on Wiley Online Library for rules of use; OA articles are governed by the applicable Creative Commons License

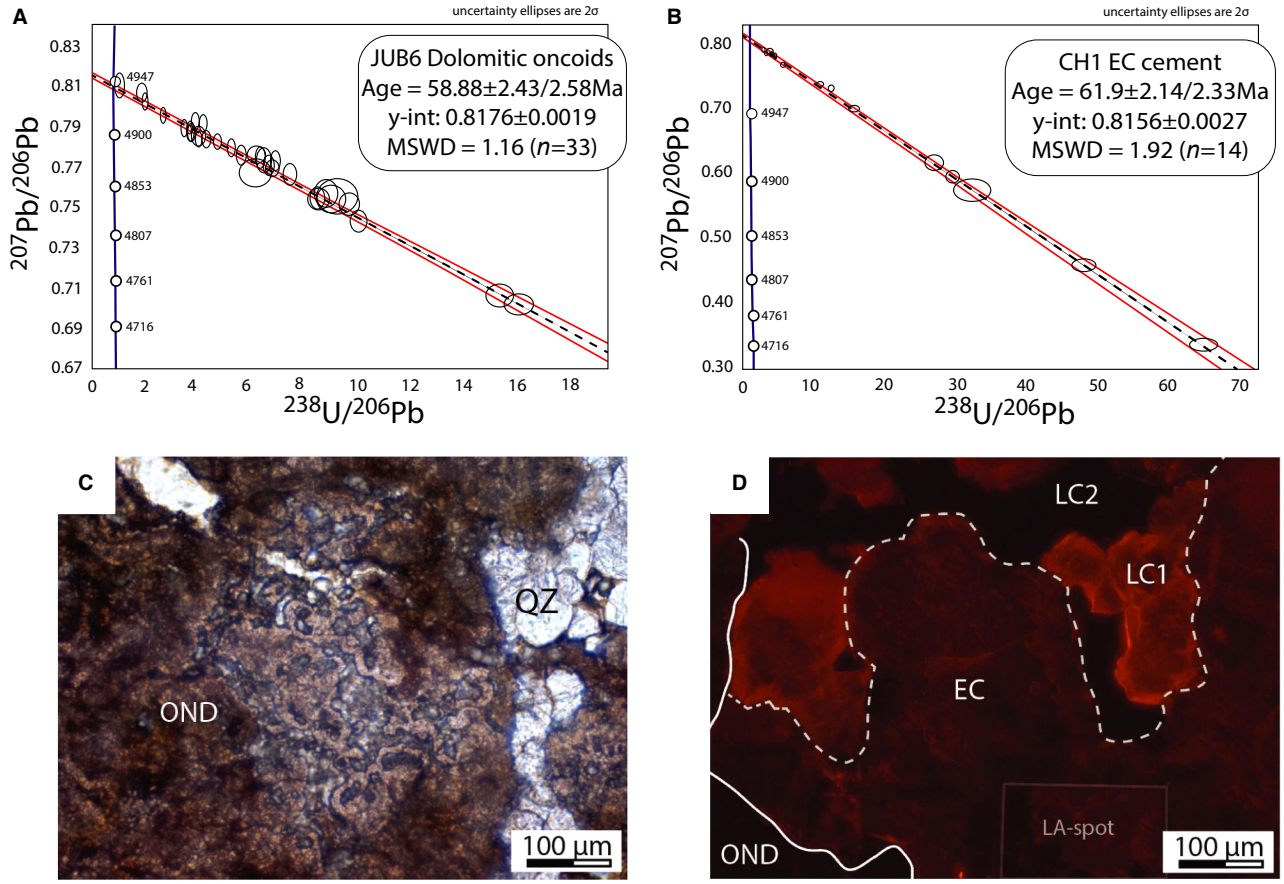

Fig. 9. $^{238}U/^{206}Pb$ versus $^{207}Pb/^{206}Pb$ Tera-Wasserburg Concordia diagrams and petrographic details of the two carbonate samples which record younger ages. (A) and (B) $^{238}U/^{206}Pb$ versus $^{207}Pb/^{206}Pb$ Tera-Wasserburg Concordia diagram and corresponding absolute ages of the dolomitic oncoids from JUB6 sample and the EC calcite from CH1. Data point error ellipses indicate 2σ internal uncertainty (95% confidence) of the isotope ratios on '*n*' analyses. Red lines represent the envelopes of the regression lines (isochrons). In blue are the Concordia curves. (C) Petrographic image illustrating the internal structure of dolomitic oncoids (OND) with microporous cores. JUB6 sample, oncoid rudstone, PPL view. (D) Dolomitic oncoids (OND) cemented by three spatially close calcite generations. The blocky calcite with dull orange zoned luminescence (EC) is post-dated by two blocky calcites (LC1 and LC2) which are bright orange and non-luminescent, respectively. The trace of a LA-spot is also illustrated. CH1, oncoidal rudstone, CL view.

possibly due to recrystallization, a process commonly occurring in early dolomites (Kupecz & Land, 1994; Machel, 1997; Elisha *et al.*, 2021). This phase was selected for U-Pb geochronology since petrographic analysis did not reveal clear petrographic hints for recrystallization (e.g. Montañez & Read, 1992; Kaczmarek & Sibley, 2014) and the oncoids displayed good preservation of their internal structure (Fig. 9C). However, the resulting age reflects the effect of recrystallization during early burial possibly driven by the oncoid microporous cores (Fig. 9C). Conversely, the young age of the blocky EC cement from CH1 sample (Fig. 9B) is possibly due to the close occurrence of this phase with two later blocky calcite cements (LC1 and LC2; Fig. 9D). These later cements possibly also occurred deeper in the thin section, below the targeted EC cement, and were also sampled by the laser.

In order to construct a CDA depth model all the dated carbonate phases ($n = 19$) were initially considered. Then, weighted average ages (CDAw) were computed from carbonate phases occurring in the same layer (Fig. 8B). Prerequisite to adopt this approach is that each CDAw derives from a single CDA population. The MSWD parameter is used to evaluate the consistency of ages from carbonate phases that should record the same geological event. It was stated that the CDAw obtained from different

© 2022 The Authors. *Sedimentology* published by John Wiley & Sons Ltd on behalf of International Association of Sedimentologists, *Sedimentology*, **69**, 2507–2534

13653091, 2022, 6, Downloaded from https://onlinelibrary.wiley.com/doi/10.1111/sed.13000 by Ifp Energies Nouvelles, Wiley Online Library on [17/01/2023]. See the Terms and Conditions (https://onlinelibrary.wiley.com/terms-and-conditions) on Wiley Online Library for rules of use; OA articles are governed by the applicable Creative Commons License

age populations result in MSWD ≫1 (Horstwood *et al.*, 2016). The application of the weighted average statistics to the Yacoraite Formation dataset allowed to discard the two younger ages previously discussed (Fig. 9). Indeed, the CDAw calculated for JUB6 and CH1 samples by also including the two younger ages resulted in MSWD >6. Consequently, the younger ages were rejected and the weighted average ages recalculated. As such the CDA depth model was derived from 17 carbonate phases for which the calculated CDAw (n = 8) satisfy the above MSWD criterion. The eight CDAw used for the model (Fig. 8B) are included between 66.60 ± 1.50 Ma (sample JUB7; n = 2; MSWD = 1.4) and 63.10 ± 1.40 Ma (sample JURD3; n = 2; MSWD = 0.02).

The assumed lack of hiatuses >0.1 to 0.4 Ma along the stratigraphic section investigated (Deschamps *et al.*, 2020) and the overall linear distribution of the CDAw, allow a linear interpolation (e.g. Watson *et al.*, 2017) to derive a CDA depth model. By applying the same procedure as for the ZDA depth model, the stratigraphically lowest and highest carbonate samples dated (i.e. JUB5, 65 m above SB1 and JURD3, 20 m below SB5; Table 1) were used to estimate the onset and end of sedimentation. Sedimentation rates of 42 m Ma^{-1} and 15 m Ma^{-1} were calculated for sequences 1 and 4 via the CDA depth model (Fig. 8C). Accordingly, the onset and end of sedimentation were respectively estimated at 67. 9 ± 1.7 Ma and 61.9 ± 1.2 Ma.

The novel approach presented allowed defining a CDA depth model for the Yacoraite Formation solely based on LAcarb ages that is consistent with biostratigraphic constraints (e.g. Moroni, 1982, 1984; Volkheimer *et al.*, 2006; Valais & Cónsole-Gonella, 2019). The model temporal resolution achieved is between 2.0% and 2.6% (2σ) and agrees with the known precision of the LAcarb technique (down to 2.0% and 1.4%, 2σ, respectively from Guillong *et al.*, 2020 and Montano *et al.*, 2021).

ZDA versus CDA depth models

The Yacoraite Formation affords the opportunity to build two depositional age depth models, one derived from zircon geochronology (ZDA depth model; Fig. 7) and the other from LAcarb (CDA depth model; Fig. 8). Zircon geochronology, a well-established chronostratigraphic tool for continental depositional systems, served as a robust framework to evaluate the reliability of the newly proposed LAcarb based age depth model. The two models were used to calculate the compacted sedimentation rates between adjacent pairs of dated layers, as well as the ages of the five sequence boundaries (SB1 to SB5) and the duration of the four third-order stratigraphic sequences that compose the Yacoraite Formation (Figs 7B and 8C).

The two models overlap with excellent agreement (Figs 7 and 8). Sequence 1 yields sedimentation rates of 32 m Ma^{-1} and 42 m Ma^{-1}, respectively, from ZDA and CDA depth models, which agree with the long transgressive trend established for sequence 1 (Deschamps *et al.*, 2020). In sequences 2 and 3, the sedimentation rates progressively increased, with mean values of 94 to 125 m Ma^{-1} in sequence 2 and 126 to 260 m Ma^{-1} in sequence 3. At SB3 sedimentation rates reach their maximum peak, with values up to 150 m Ma^{-1} and 330 m Ma^{-1}, respectively (Figs 7B and 8B). This peak is in line with a pulse of carbonate production and sediment supply known for this stratigraphic interval (Rohais *et al.*, 2019). The higher sedimentation rates recorded in sequence 3 by the LAcarb model (Fig. 8C) may be due to a Sadler effect (i.e. changes in the sedimentation rate estimations depending on the vertical distribution and uncertainty of the ages; Sadler, 1981), which is induced by the presence of only one sample analyzed between 70 m and 180 m (i.e. JUR25; CDAw = 64.10 ± 2.30 Ma, n = 2; MSWD = 0.2). Starting from SB4 the sedimentation rates decreased down to 20 m Ma^{-1} and 15 m Ma^{-1}, respectively. This agrees with the depositional system of sequence 4 being characterized by multiple emersion events that culminated in a major exposure in correspondence with SB5 (Deschamps *et al.*, 2020). The sedimentation rates calculated for each stratigraphic sequence represent mean estimates and may vary according to the vertical distribution and age uncertainty of the dated samples. As such, the values obtained by the two models may differ (for example, sequence 3) although they describe the same sedimentation rate dynamics.

Sequence boundary ages estimated from the two models are consistent within uncertainties, although those inferred via LAcarb are on average 0.4 Ma younger (Fig. 8A). This reflects the notion of minimum age estimate provided by carbonates related to early diagenetic modifications. LAcarb ages are also less precise than zircon ages so that ZDA and CDA depth models

© 2022 The Authors. *Sedimentology* published by John Wiley & Sons Ltd on behalf of International Association of Sedimentologists, *Sedimentology*, **69**, 2507–2534

13653091, 2022, 6, Downloaded from https://onlinelibrary.wiley.com/doi/10.1111/sed.13000 by Ifp Energies Nouvelles, Wiley Online Library on [17/01/2023]. See the Terms and Conditions (https://onlinelibrary.wiley.com/terms-and-conditions) on Wiley Online Library for rules of use; OA articles are governed by the applicable Creative Commons License

provide precision of *ca* 0.9 to 1.4% and *ca* 2.0 to 2.6%, respectively (Figs 7 and 8).

Ages of SB1 and SB5 were inferred from both models (Figs 7 and 8). Accordingly, the Yacoraite Formation was deposited between 68.1 ± 0.9 Ma and 62.3 ± 0.6 Ma and between 67.9 ± 1.7 Ma to 61.9 ± 1.3 Ma, respectively, from ZDA and CDA depth models. Thus, the total sedimentation duration inferred is *ca* 5.7 Ma and *ca* 6.0 Ma. It is therefore possible to assess that sedimentation started at *ca* 68 Ma during Maastrichtian time and ended at *ca* 62 Ma during Danian time. These results agree with the occurrence of Maastrichtian dinosaur footprints in sequence 2 of the Yacoraite Formation which are not recorded in the youngest sequences (Cónsole-Gonella *et al.*, 2017) and of Danian palynomorphs in the overlying Tunal Formation (Volkheimer *et al.*, 2006).

The duration of the four third-order stratigraphic sequences, which compose the Yacoraite Formation (Figs 7 and 8), span from 0.7 Ma (sequence 3) to 2.8 Ma (sequence 1) based on zircon geochronology and from 0.4 Ma (sequence 3) to 2 Ma (sequence 4) based on LAcarb data. This supports the third-order cyclicity (i.e. cycle duration of 0.5 to 5 Ma; Van Wagoner *et al.*, 1988) recorded in the Yacoraite Formation by previous authors (Marquillas, 1985; Salfity & Marquillas, 1994; Hernandez *et al.*, 1999; Rohais, *et al.*, 2019; Deschamps *et al.*, 2020).

Carbonate dating potential: insights from the Yacoraite Formation

The excellent match between the ZDA and CDA depth models from the Yacoraite Formation (Fig. 8A), together with their consistency with the available biostratigraphic constraints, suggest that LAcarb may be used as a reliable chronostratigraphic tool to compute robust depositional age depth models. However, limitations of this tool require to be better understood for reliable applications in settings that lack independent chronostratigraphic constraints (for example, zircon ash layer ages). The term dating potential refers to the probability to produce accurate and precise ages. Evaluating the dating potential requires to establish: (i) the dating success rate (i.e. the percentage of samples providing accurate ages); and (ii) the time resolution of the method (i.e. the age precision). These parameters mainly depend on the sensitivity of carbonates to diagenetic modifications and to the original U-Pb carbonate composition.

Carbonates are sensitive to textural and geochemical changes due to diagenesis, potentially causing age resetting (Jones *et al.*, 1995; Kelly *et al.*, 2003; Li *et al.*, 2014; Roberts *et al.*, 2020a). Consequently, depositional and early diagenetic carbonates may easily provide younger ages, recording the timing of later diagenetic modifications (e.g. Jones *et al.*, 1995; Li *et al.*, 2014; Mangenot *et al.*, 2018; Roberts *et al.*, 2020a; Brigaud *et al.*, 2021). Carbonate grains and cements originally precipitated with an unstable mineralogy (i.e. aragonite, high-Mg calcite and dolomite) are more prone to undergo these modifications and are usually associated with a lower dating potential (Li *et al.*, 2014; Brigaud *et al.*, 2021; Elisha *et al.*, 2021). However, grains and cements with stable mineralogy may also be exposed to diagenesis if they are characterized by high reactive surfaces (function of their coarseness) or if they occur in permeable carbonate facies that favour post-depositional fluid migrations.

Although diagenesis plays an important role on the dating potential, this is strongly linked to the pristine U-Pb composition of carbonates. The latter in turn depends on the environmental conditions and processes driving precipitation. Statistically robust lower intercept U-Pb ages are calculated from carbonates that initially incorporated high and variable amounts of U and low and homogeneous amounts of Pb (Rasbury & Cole, 2009). However, while the initial heterogeneity of the U/Pb ratios matters, the U concentration is the main dating potential limitation (Rasbury *et al.*, 2021). The mechanisms for U incorporation are not well-understood because they rely on many factors. These include U and Pb availability in the fluid, mineralogy, carbonate type, growth rate, temperature, pH, Eh, pCO_2, Ca^{2+}/CO_3^{2-} ratio, U complexation, organic matter degradation and microbial activity (Kelly *et al.*, 2003; Cole *et al.*, 2004; Tribovillard *et al.*, 2006; Miyajima *et al.*, 2021; Roberts *et al.*, 2021). Although the interplay between these factors remains unclear, carbonates precipitated from lacustrine water, meteoric water and groundwater are particularly amenable to dating (e.g. Rasbury & Cole, 2009; Drost *et al.*, 2018; Liivamägi *et al.*, 2018; Frisch *et al.*, 2019; Parrish *et al.*, 2019; Woodhead & Petrus, 2019; Kurumada *et al.*, 2020; Nicholson *et al.*, 2020; Roberts *et al.*, 2020a, 2021; Brigaud *et al.*, 2021; Hoareau *et al.*, 2021; Montano *et al.*, 2021; Nuriel *et al.*, 2021; Rasbury *et al.*, 2021).

The Yacoraite Formation lacustrine carbonates proved to have a good dating potential. Indeed, 17

© 2022 The Authors. *Sedimentology* published by John Wiley & Sons Ltd on behalf of International Association of Sedimentologists, *Sedimentology*, **69**, 2507–2534

13653091, 2022, 6, Downloaded from https://onlinelibrary.wiley.com/doi/10.1111/sed.13000 by Ifp Energies Nouvelles, Wiley Online Library on [17/01/2023]. See the Terms and Conditions (https://onlinelibrary.wiley.com/terms-and-conditions) on Wiley Online Library for rules of use; OA articles are governed by the applicable Creative Commons License

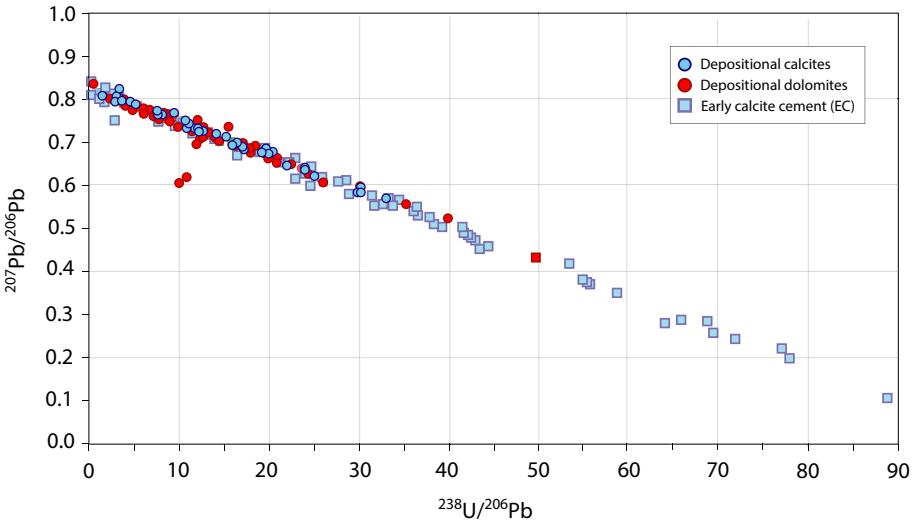

Fig. 10. Cross-plot of $^{238}U/^{206}Pb$ versus $^{207}Pb/^{206}Pb$ ratios of the 17 carbonate phases used to build the CDA depth model. Each dot corresponds to an ablation analysis. Depositional carbonates (microbialites, ooids and oncoids) are grouped together and distinguished based on their mineralogy (calcite in blue versus dolomite in red). The early calcite cement (EC) is represented by light blue squares.

over the 22 carbonate phases analyzed (77%) yielded ages consistent with those from zircon geochronology (Figs 6 and 8A; Appendix S2). Two phases gave ages younger than deposition (Fig. 9) and only three phases were unsuitable for dating (Pb >10 ppm and U <7 ppm; Appendix S1). The achieved age precision is down to 1.4% (2σ). The quality of these results, both in terms of accuracy and precision, was favoured by various factors. Depositional and early diagenetic carbonates of the Yacoraite Formation from the Metán and Alemania sub-basins were only locally overprinted by burial diagenesis and mostly preserved pristine geochemical features (Sial *et al.*, 2001; Durieux & Brown, 2007; Marquillas *et al.*, 2007; Rohais *et al.*, 2019; Gomes *et al.*, 2020). Consequently, the C and O isotope signatures of these carbonates have been used to reconstruct the evolution of the lacustrine water composition (Sial *et al.*, 2001; Marquillas *et al.*, 2007; Rohais *et al.*, 2019). Additionally, the original U and Pb geochemistry of the investigated carbonates played an important role in the dating potential. The Juramento stratigraphic section is located close to a basin depocentre (Fig. 1; Deschamps *et al.*, 2020) where the input of terrigenous clays, commonly rich in Pb, was limited. This is of great importance since high Pb concentrations negatively affects the feasibility of dating. In parallel, the suitable U concentration of the investigated carbonates could have been promoted by the widespread microbial activity characterizing the whole deposition of the Yacoraite Formation (Deschamps *et al.*, 2020; Gomes *et al.*, 2020). This is known to play a pivotal role in the incorporation of U via processes of direct enzymatic reduction, biosorption, biomineralization and bioaccumulation (e.g. Cole *et al.*, 2004; McManus *et al.*, 2006; Tribovillard *et al.*, 2006). Despite these common conditions controlling the general availability and incorporation of U and Pb, the different carbonate phases analyzed provided variable age precisions (Table 1; Fig. 6; Appendix S2). In particular, the early lacustrine cement (EC) yielded the highest age precision with uncertainties down to 1.4% (2σ). This cement showed the ideal composition for dating with heterogeneous $^{238}U/^{206}Pb$ values bracketed between 0.2 and 89 (Fig. 10) and U and Pb concentrations up to 7.3 ppm and 3.1 ppm, respectively. It precipitated early within the interparticle and framework pores of the carbonates. Here the relatively more reducing conditions, due to the limited connection with the lacustrine waters above the sediment–water interface, may have favoured U incorporation. Furthermore, this cement consists of coarse blocky crystals of low-Mg calcite. The low reactive surface and stable mineralogy possibly prevented diagenesis to alter the initial favourable composition. Contrarily, depositional carbonates (i.e. microbialites, ooids and oncoids) provided a slightly lower age precision with uncertainties from 1.7 to 16% (2σ). These phases are

© 2022 The Authors. *Sedimentology* published by John Wiley & Sons Ltd on behalf of International Association of Sedimentologists, *Sedimentology*, **69**, 2507–2534

13653091, 2022, 6, Downloaded from https://onlinelibrary.wiley.com/doi/10.1111/sed.13000 by Ifp Energies Nouvelles, Wiley Online Library on [17/01/2023]. See the Terms and Conditions (https://onlinelibrary.wiley.com/terms-and-conditions) on Wiley Online Library for rules of use; OA articles are governed by the applicable Creative Commons License

characterized by more homogeneous $^{238}U/^{206}Pb$ values, mostly between 0.5 and 30 (Fig. 10), and an overall higher Pb concentration (up to 10 ppm). The microbial communities that are known to induce and/or influence the precipitation of these carbonate phases may have trapped fine-grained detrital material such as clays (e.g. Suarez-Gonzalez *et al.*, 2019) accounting for the Pb enrichment. Additionally, the high microporosity (and reactive surface) associated with these carbonates could have induced syn-depositional fluid–rock interactions and consequent lower age precision.

Strategy for building CDA depth models

To maximize the chances to obtain a reliable depositional age depth model based on LAcarb, a working strategy is here proposed. This strategy consists of the following steps: (i) choice of stratigraphic section and samples; (ii) sample petrography and geochemistry; (iii) LAcarb feasibility screening; and (iv) weighted average statistics and data interpolation.

Choice of stratigraphic section and samples

Stratigraphic sections that suffered severe burial diagenesis, fracturing, hydrothermalism and/or hosting ore mineralization should be avoided, since the carbonates could possibly record the timing of later fluid-flow events rather than of deposition.

The frequency of sampling along the section has to be carefully evaluated after a preliminary sedimentological analysis. The availability of carbonate layers along the section, the occurrence of possible emersion surfaces and related sedimentary hiatuses and the sedimentation rate evolution should be taken into consideration. Intervals characterized by high sedimentation rates will require lower sampling frequency than those with low sedimentation rates.

The layers to be sampled should be those where various coeval carbonate types coexist (for example, ooids, microbialite, oncoids, bioclasts and cements). This will allow dating multiple phases that represent the same geological event (i.e. deposition) and potentially will give a single age population. This choice may be dictated also by the presumed dating potential of the different carbonates (see previous section). Therefore, bioclasts that are known to precipitate with aragonite or high-Mg calcite mineralogy and carbonate mud characterized by high reactive surface, should be avoided.

Sample petrography and geochemistry

A petrographic characterization is of primary importance to select depositional and early diagenetic carbonates that will most possibly provide depositional ages. The diagenetic overprinting of these carbonates may be inferred, among others from: (i) the staining and CL response (Dickson, 1966; Machel, 2000) revealing ferroan versus non-ferroan composition; (ii) the coarseness of micrite crystals (e.g. Deville de Periere *et al.*, 2011) revealing possible recrystallization; (iii) the obliteration of primary features (for example, concentric and radial crystal arrangement in ooids; Simone, 1980); and (iv) the occurrence of pervasive chemical compaction features (for example, stylolitization).

Despite the quality of the petrographic work, carbonate phases altered by later diagenesis may be erroneously chosen. This was the case for the dolomitic oncoids from the JUB6 sample (Fig. 9). Geochemical analysis accomplished in parallel of the petrographic work can mitigate selecting altered carbonate phases. Carbon, oxygen and strontium isotopes provide insights on the sample palaeoenvironment and diagenetic history (e.g. Talbot, 1990; Swart, 2015). In marine contexts the preservation of pristine geochemical compositions of carbonates may be tested by evaluating the consistency of the $\delta^{18}O$, $\delta^{13}C$ and $^{87}Sr/^{86}Sr$ measured with those of coeval carbonates from global chemostratigraphic curves (e.g. Veizer *et al.*, 1999). Elemental geochemistry of depositional and early diagenetic carbonates commonly reveals lower Fe-Mn and higher Sr-Na contents compared to carbonates precipitated or modified during burial (Kretz, 1982; Veizer, 1983; Barnaby & Rimstidt, 1989). Geochemical maps may also be useful to evaluate the compositional consistency among coeval carbonate phases (e.g. Drost *et al.*, 2018).

LAcarb feasibility screening

Despite the efforts made in the previous steps to select the carbonate phases to be dated, the complexity of U-Pb incorporation and the diagenetic disturbance in carbonates may result in unpredictable low dating potential even in ideal carbonates. Consequently, it is highly encouraged to perform a LAcarb screening on a few samples to evaluate the dating feasibility (i.e. presence of suitable U-Pb composition) and the quality of the achievable ages. Afterwards, LAcarb analytical sessions on the whole sample set may be performed by following the method reported in this study (Ring & Gerdes, 2016) or those adopted by other

© 2022 The Authors. *Sedimentology* published by John Wiley & Sons Ltd on behalf of International Association of Sedimentologists, *Sedimentology*, **69**, 2507–2534

13653091, 2022, 6, Downloaded from https://onlinelibrary.wiley.com/doi/10.1111/sed.13000 by Ifp Energies Nouvelles, Wiley Online Library on [17/01/2023]. See the Terms and Conditions (https://onlinelibrary.wiley.com/terms-and-conditions) on Wiley Online Library for rules of use; OA articles are governed by the applicable Creative Commons License

laboratories (e.g. Roberts & Walker, 2016; Nuriel *et al.*, 2021).

Weighted average statistics and data interpolation

Due to the issue of diagenesis, one U-Pb age is commonly not sufficient to reliably inform on the depositional age of the sampled layer. To provide more robust time constraints for deposition, it is here proposed to calculate weighted average ages (CDAw) from depositional and early diagenetic carbonates coexisting in the same layer. When the CDAw obtained are characterized by MSWD $\gg$1 it is suggested to reject the younger ages (see section *CDA depth model from carbonate geochronology*). If all of the carbonate phases analyzed in the layer have been reset by the same event of post-depositional diagenesis, the resulting CDAw would satisfy the MSWD criterion and erroneously considered to construct the age depth model. This CDAw may however cause an age reversal in the model and could thus *a posteriori* be discarded from the dataset by applying the principle of superposition.

Once the weighted average ages have been obtained and possible outliers eliminated, data interpolation has to be performed in order to build the CDA depth model. The choice of the interpolation approach relies on the distribution of the ages along the section and the occurrence and duration of possible hiatuses. Linear data interpolation (e.g. Watson *et al.*, 2017) is recommended when ages are linearly distributed and major hiatuses do not occur along the section. Conversely, more complex LAcarb dataset (for example, numerous ages, variable uncertainties and presence of hiatuses) would require other interpolation methods (e.g. Blaauw, 2010; Blaauw *et al.*, 2012, 2018; Lougheed & Obrochta, 2019).

The strategy proposed here may be of valuable help for future LAcarb applications and can be adopted in various geological contexts, from marine to continental. Therefore, LAcarb can integrate the current chronostratigraphy toolbox and be used to build depositional age depth models and evaluate the sedimentation rate dynamics in settings with otherwise poor time constraints for deposition.

CONCLUSIONS

The Yacoraite Formation (Maastrichtian–Danian, Salta rift basin), composed by lacustrine deposits with interbedded volcanic ashes and organized in four third-order stratigraphic sequences, represents an ideal target to validate the reliability of carbonate U-Pb geochronology for chronostratigraphic studies. Two depositional age depth models were constrained via zircon and carbonate U-Pb geochronology along the same stratigraphic section. Zircon geochronology produced ages that get younger up-section (between 67.55 ± 0.89 Ma and 63.33 ± 0.56 Ma) and were linearly interpolated to derive a depositional model with a precision of 0.9 to 1.4% (2σ).

Lacustrine carbonates, including microbialites, ooids, oncoids and early cements, were dated. A novel approach to develop a depositional model via LAcarb was implemented: weighted average ages (between 66.60 ± 1.50 Ma and 63.10 ± 1.40 Ma) were derived from dated carbonate phases coexisting in the same layer and were then linearly interpolated along the section. The model provided a precision of 2 to 2.6% (2σ).

The two models exhibit excellent overlap and suggest that sedimentation started at *ca* 68 Ma and ended at *ca* 62 Ma, in agreement with biostratigraphic constraints. The sedimentation rates calculated from the two models agree with sedimentological and stratigraphic evidence. In addition, the duration inferred for the four third-order stratigraphic sequences (0.4 to 2.1 Ma) is consistent with the known third-order cyclicity of the Yacoraite Formation. A versatile working strategy is proposed to overcome the main LAcarb limitations (i.e. carbonate composition and diagenesis) and to build reliable LAcarb-based depositional age models.

Results from this study show that, with the favourable samples and a suitable working strategy, carbonate U-Pb geochronology can be reliably used to provide depositional ages at the resolution of the third-order stratigraphic sequence. This is particularly relevant to reconstruct chronostratigraphy and sedimentation rate dynamics of hardly dateable sedimentary rocks that are not amenable to other geochronological tools.

ACKNOWLEDGEMENTS

This research was undertaken during D. Montano PhD project, funded by IFP Energies nouvelles. This is FIERCE contribution No. 97. FIERCE is financially supported by the Wilhelm and Else Heraeus Foundation and by the Deutsche Forschungsgemeinschaft (DFG, INST

© 2022 The Authors. *Sedimentology* published by John Wiley & Sons Ltd on behalf of International Association of Sedimentologists, *Sedimentology*, **69**, 2507–2534

13653091, 2022, 6, Downloaded from https://onlinelibrary.wiley.com/doi/10.1111/sed.13000 by Ifp Energies Nouvelles, Wiley Online Library on [17/01/2023]. See the Terms and Conditions (https://onlinelibrary.wiley.com/terms-and-conditions) on Wiley Online Library for rules of use; OA articles are governed by the applicable Creative Commons License

161/921-1 FUGG and INST 161/923-1 FUGG), which is gratefully acknowledged. We are grateful for the scientific exchange with Prof. J.L. Paquette. We thank Thin Section Lab (TSL) for high quality thin section manufacturing. The manuscript benefitted of significant improvements from the careful revisions of Prof. David Chew, an anonymous reviewer, the chief editor Dr Alex Brasier and the associated editor Prof. Mike Rogerson. Open Access Funding provided by Universita degli Studi di Milano within the CRUI-CARE Agreement.

CONFLICT OF INTEREST

The authors know of no conflict of interest in connection with this work.

DATA AVAILABILITY STATEMENT

Data to support this study are available in the supplementary material.

REFERENCES

Alonso, R.N. and **Marquillas, R.A.** (1986) Nueva localidad con huellas de dinosaurios y primer hallazgo de huellas de aves en la Formacion Yacoraite (Maastrichtiano) del Norte Argentino. 2. Actas. 4th Congr. Arg. Paleont. Bioestrat., 33–41.

Barnaby, R.J. and **Rimstidt, J.D.** (1989) Redox conditions of calcite cementation interpreted from Mn and Fe contents of authigenic calcites. *Geol. Soc. Am. Bull.*, **101**, 795–804.

Bento-Freire, E. (2012) High Resolution Sequence Stratigraphic characterization of microbial carbonate from Palaeocene interval of Yacoraite Formation – Argentine. Master Thesis, Federal Univ. Rio de Janeiro, Rio de Janeiro (in Portuguese with English abstract).

Berra, F. and **Carminati, E.** (2010) Subsidence history from a backstripping analysis of the Permo-Mesozoic succession of the Central Southern Alps (Northern Italy). *Basin Res.*, **22**, 952–975.

Bilau, A., **Rolland, Y.**, **Schwartz, S.**, **Godeau, N.**, **Guihou, A.**, **Deschamps, P.**, **Brigaud, B.**, **Noret, A.**, **Dumont, T.** and **Gautheron, C.** (2021) Extensional reactivation of the Penninic Frontal Thrust 3 Ma ago as evidenced by U-Pb dating on calcite in fault zone cataclasite. *Solid Earth*, **12**, 237–251.

Blaauw, M. (2010) R-Code for 'classical' age-modelling (CLAM V1.0) of radiocarbon sequences. *PANGAEA*, https://doi.org/10.1594/PANGAEA.873023.

Blaauw, M., **Christen, J.**, **Bennett, K.** and **Reimer, P.** (2018) Double the dates and go for Bayes — impacts of model choice, dating density and quality on chronologies. *Quat. Sci. Rev.*, **188**, 58–66.

Blaauw, M., **Holliday, V.T.**, **Gill, J.L.** and **Nicoll, K.** (2012) Age models and the Younger Dryas Impact Hypothesis. *Proc. Natl Acad. Sci. USA*, **109**(34), E2240.

Bohacs, K.M., **Carroll, A.R.**, **Neal, J.E.** and **Mankiewicz, P.J.** (2000) Lake-basin type, source potential, and hydrocarbon character: an integrated-sequence-stratigraphic–geochemical framework. In: *Lake Basins through Space and Time: AAPG Studies in Geology*, Vol. **46** (Eds Gierlowski-Kordesch, E.H. and Kelts, K.R. eds.), pp. 3–34. American Association of Petroleum Geologists (AAPG), Tulsa.

Brigaud, B., **Andrieu, S.**, **Blaise, T.**, **Haurine, F.** and **Barbarand, J.** (2021) Calcite uranium–lead geochronology applied to hardground lithification and sequence boundary dating. *Sedimentology*, **68**, 168–195.

Cartier, R., **Brisset, E.**, **Guiter, F.**, **Sylvestre, F.**, **Kazuyo, T.**, **Anthony, E.J.**, **Paillès, C.**, **Bruneton, H.**, **Bard, E.** and **Miramont, C.** (2018) Multiproxy analyses of Lake Allos reveal synchronicity and divergence in geosystem dynamics during the Lateglacial/Holocene in the Alps. *Quat. Sci. Rev.*, **186**, 60–77.

Ceraldi, S.T. and **Green, D.** (2016) Evolution of the South Atlantic lacustrine deposits in response to Early Cretaceous rifting, subsidence and lake hydrology. *Geol. Soc. Spec. Publ.*, **438**, 77–98.

Cesaretti, N.N., **Parnell, J.** and **Dominguez, E.A.** (2000) Pore fluid evolution within a hydrocarbon reservoir: Yacoraite formation (Upper Cretaceous), Northwest Basin, Argentina. *J. Petrol. Geol.*, **23**, 375–398.

Cole, J.M., **Rasbury, E.T.**, **Montañez, I.P.**, **Pedone, V.A.**, **Lanzirotti, A.** and **Hanson, G.N.** (2004) Petrographic and trace element analysis of uranium-rich tufa calcite, middle Miocene Barstow Formation, California, USA: uranium-rich tufa deposits, California. *Sedimentology*, **51**, 433–453. https://doi.org/10.1111/j.1365-3091.2004.00631.x.

Cónsole-Gonella, C., **de Valais, S.**, **Marquillas, R.A.** and **Sánchez, M.C.** (2017) The Maastrichtian-Danian Maimará tracksite (Yacoraite Formation, Salta Group), Quebrada de Humahuaca, Argentina: environments and ichnofacies implications. *Palaeogeogr. Palaeoclimatol. Palaeoecol.*, **468**, 327–350.

Crombez, V., **Rohais, S.**, **Euzen, T.**, **Riquier, L.**, **Baudin, F.** and **Hernandez-Bilbao, E.** (2020) Trace metal elements as paleoenvironmental proxies: why should we account for sedimentation rate variations? *Geology*, **48**(8), 839–843.

Cruset, D., **Vergés, J.**, **Albert, R.**, **Gerdes, A.**, **Benedicto, A.**, **Cantarero, I.** and **Travé, A.** (2020) Quantifying deformation processes in the SE Pyrenees using U-Pb dating of fracture-filling calcites. *J. Geol. Soc.*, **177**, 1186–1196.

Deschamps, R., **Rohais, S.**, **Hamon, Y.** and **Gasparrini, M.** (2020) Dynamic of a lacustrine sedimentary system during late rifting at the Cretaceous-Palaeocene transition: example of the Yacoraite Formation, Salta Basin, Argentina. *Depos. Rec.*, **6**, 490–523.

Deville de Periere, M., **Durlet, C.**, **Vennin, E.**, **Lambert, L.**, **Bourillot, R.**, **Caline, B.** and **Poli, E.** (2011) Morphometry of micrite particles in cretaceous microporous limestones of the Middle East: influence on reservoir properties. *Mar. Pet. Geol.*, **28**, 1727–1750.

Dickson, J.A.D. (1966) Carbonate identification and genesis as revealed by staining. *J. Sediment. Petrol.*, **36**(2), 491–505.

13653091, 2022, 6, Downloaded from https://onlinelibrary.wiley.com/doi/10.1111/sed.13000 by Ifp Energies Nouvelles, Wiley Online Library on [17/01/2023]. See the Terms and Conditions (https://onlinelibrary.wiley.com/terms-and-conditions) on Wiley Online Library for rules of use; OA articles are governed by the applicable Creative Commons License

Disalvo, A., **Hoffman, C.**, **Lúquez, J.** and **Rodríguez Schelotto, M.** (2002) Los reservorios de la Formaciónes Palmar Largo y La Tigra. In: *Rocas Reservorio De La Cuencas Productivas De La Argentina* (Eds Schiuma, M., Hinterwimmer, G. and Vergani, G.), pp. 739–752. Y Congreso de Exploración y Desarrollo de hidrocarburos, Mar del Plata.

Drost, K., **Chew, D.**, **Petrus, J.A.**, **Scholze, F.**, **Woodhead, J.D.**, **Schneider, J.W.** and **Harper, D.A.T.** (2018) An image mapping approach to U-Pb LA-ICP-MS carbonate dating and applications to direct dating of carbonate sedimentation. *Geochem. Geophys. Geosyst.*, **19**, 4631–4648.

Dunham, R.J. (1962) Classification of Carbonate Rocks according to depositional texture. In: *Classification of Carbonate Rocks* (Ed. Ham, W.E.), *AAPG Memoir.*, **1**, 108-121.

Durieux, C.G. and **Brown, A.C.** (2007) Geological context, mineralization, and timing of the Juramento sediment-hosted stratiform copper-silver deposit, Salta district, Northwestern Argentina. *Miner. Depos.*, **42**, 879–899.

Einsele, G. (2001) Sedimentary basins: evolution, facies, and sediment budget. *Sediment. Geol.*, **143**, 185–186.

Elisha, B., **Nuriel, P.**, **Kylander-Clark, A.** and **Weinberger, R.** (2021) Towards in-situ U-Pb dating of dolomites. *Geochronology*, **3**, 337–349.

Enos, P. (1991) Sedimentary parameters for computer modeling. In: *Sedimentary Modeling, Computer Simulations and Methods for Improved Parameter Definition* (Eds Franseen, E.K., Watney, W.L., Kendall, C.G.S.C. and Ross, W.), *Kansas Geol. Survey Bull.*, **233**, 63–101.

Fernandez, J. (1975) Hallazgo de peces pulmonados fosiles en la Puna Jujena. *An. Soc. Cient. Argent.*, **2**(41), 13–18.

Flügel, E. (2004) *Microfacies of carbonate rocks. Analysis, interpretation and application*. Springer, Berlin, 976 pp.

Frisch, K., **Voigt, S.**, **Verestek, V.**, **Appel, E.**, **Albert, R.**, **Gerdes, A.**, **Arndt, I.**, **Raddatz, J.**, **Voigt, T.**, **Weber, Y.** and **Batenburg, S.J.** (2019) Long-period astronomical forcing of westerlies' strength in central Asia during Miocene climate cooling. *Paleoceanogr. Paleoclimatol.*, **34**, 1784–1806.

Gebhardt, A.C., **Naudts, L.**, **De Mol, L.**, **Klerkx, J.**, **Abdrakhmatov, K.**, **Sobel, E.R.** and **De Batist, M.** (2017) High-amplitude lake-level changes in tectonically active Lake Issyk-Kul (Kyrgyzstan) revealed by high-resolution seismic reflection data. *Clim. Past*, **13**(1), 73–92.

Gerdes, A. and **Zeh, A.** (2006) Combined U-Pb and Hf isotope LA-(MC-) ICP-MS analyses of detrital zircons: comparison with SHRIMP and new constraints for the provenance and age of an Armorican metasediment in Central Germany. *Earth Planet. Sci. Lett.*, **249**, 47–61.

Gerdes, A. and **Zeh, A.** (2009) Zircon formation versus zircon alteration-new insights from combined V-Ph and Lu-Hf in situ LA-ICP-MS analyses, and consequences for the interpretation of Archean zircon from the Central Zone of the Limpopo Belt. *Chem. Geol.*, **261**(3–4), 230–243.

Gomes, J.P.B., **Bunevich, R.B.**, **Tonietto, S.N.**, **Alves, D.B.**, **Santos, J.F.** and **Whitaker, F.F.** (2020) Climatic signals in lacustrine deposits of the Upper Yacoraite Formation, Western Argentina: evidence from clay minerals, analcime, dolomite and fibrous calcite. *Sedimentology*, **67**, 2282–2309.

Gómez-Omil, R.J., **Boll, A.** and **Hernández, R.M.** (1987) Cuenca cretácico-terciaria del Noroeste argentino (Grupo Salta). In: *X Congr. Geol. Argent., 5, Tucumán*, p. 9 (inédit).

Guillong, M., **Wotzlaw, J.-F.**, **Looser, N.** and **Laurent, O.** (2020) New analytical and data evaluation protocols to improve the reliability of U-Pb LA-ICP-MS carbonate dating. https://doi.org/10.5194/gchron-2019-20

Hernandez, R., **Disalvo, A.**, **Boll, A.** and **Gomez Omil, R.** (1999) Sequence Stratigraphy of Salta Group, focusing at sub-basins Metán-Alemania, Northwest Argentine. In: *Congreso geologico argentino* (Eds González Bonorino, G., Omarini y, R. and Viramonte, J.), pp. 264–284. Nacional Univ. Salta, Salta.

Hoareau, G., **Claverie, F.**, **Pecheyran, C.**, **Paroissin, C.**, **Grignard, P.**, **Motte, G.**, **Chailan, O.** and **Girard, J.** (2021) Direct U-Pb dating of carbonates from micron-scale femtosecond laser ablation inductively coupled plasma mass spectrometry images using robust regression. *Geochronology*, **3**, 67–87.

Hopley, P.J., **Reade, H.**, **Parrish, R.**, **De Kock, M.** and **Adams, J.W.** (2019) Speleothem evidence for C3 dominated vegetation during the Late Miocene (Messinian) of South Africa. *Rev. Palaeobot. Palynol.*, **264**, 75–89.

Horstwood, M.S.A., **Košler, J.**, **Gehrels, G.**, **Jackson, S.E.**, **McLean, N.M.**, **Paton, C.**, **Pearson, N.J.**, **Sircombe, K.**, **Sylvester, P.**, **Vermeesch, P.**, **Bowring, J.F.**, **Condon, D.J.** and **Schoene, B.** (2016) Community-derived standards for LA-ICP-MS U-(Th-)Pb geochronology – uncertainty propagation, age interpretation and data reporting. *Geostand. Geoanal. Res.*, **40**, 311–332.

Jackson, S.E., **Pearson, N.J.**, **Griffin, W.L.** and **Belousova, E.A.** (2004) The application of laser ablation-inductively coupled plasma-mass spectrometry to in situ U-Pb zircon geochronology. *Chem. Geol.*, **211**(1–2), 47–69.

Jones, C.E., **Halliday, A.N.** and **Lohmann, K.C.** (1995) The impact of diagenesis on high-precision UPb dating of ancient carbonates: an example from the Late Permian of New Mexico. *Earth Planet. Sci. Lett.*, **134**(3–4), 409–423.

Kaczmarek, S.E. and **Sibley, D.F.** (2014) Direct physical evidence of dolomite recrystallization. *Sedimentology*, **61**, 1862–1882.

Kamenetsky, V., **Belousova, E.**, **Giuliani, A.**, **Kamenetsky, M.**, **Goemann, K.** and **Griffin, W.** (2014) Chemical abrasion of zircon and ilmenite megacrysts in the Monastery kimberlite: implications for the composition of kimberlite melts. *Chem. Geol.*, **383**, 76–85.

Katz, B. (2001) Lacustrine basin hydrocarbon exploration – current thoughts. *J. Paleolimnol.*, **26**, 161–179.

Kelly, S.D., **Newville, M.**, **Cheng, L.R.**, **Kemner, K.M.**, **Sutton, S.R.**, **Fenter, P.**, **Sturchio, N.C.** and **Spötl, C.** (2003) Uranyl incorporation in natural calcite. *Environ. Sci. Technol.*, **37**, 1284–1287.

Kelts, K. and **Talbot, M.** (1990) Lacustrine carbonates as geochemical archives of environmental change and biotic/abiotic interactions. In: *Large Lakes. Brock/Springer Series in Contemporary Bioscience* (Eds Tilzer, M.M. and Serruya, C.), pp. 288–315. Springer, Berlin, Heidelberg.

Kretz, R. (1982) A model for the distribution of trace elements between calcite and dolomite. *Geochim. Cosmochim. Acta*, **46**(10), 1979–1981.

Kupecz, J.A. and **Land, L.S.** (1994) Progressive recrystallization and stabilization of early-stage dolomite: Lower Ordovician Ellenburger Group, West Texas. In: *Dolomites: A Volume in Honour of Dolomieu* (Eds Purser, B., Tucker, M. and Zenger, D.), pp. 255–279. Blackwell

© 2022 The Authors. *Sedimentology* published by John Wiley & Sons Ltd on behalf of International Association of Sedimentologists, *Sedimentology*, **69**, 2507–2534

13653091, 2022, 6, Downloaded from https://onlinelibrary.wiley.com/doi/10.1111/sed.13000 by Ifp Energies Nouvelles, Wiley Online Library on [17/01/2023]. See the Terms and Conditions (https://onlinelibrary.wiley.com/terms-and-conditions) on Wiley Online Library for rules of use; OA articles are governed by the applicable Creative Commons License

Publishing, Oxford. https://doi.org/10.1002/9781444304077.ch15

Kurumada, Y., **Aoki, S.**, **Aoki, K.**, **Kato, D.**, **Saneyoshi, M.**, **Tsogtbaatar, K.**, **Windley, B.F.** and **Ishigaki, S.** (2020) Calcite U-Pb age of the cretaceous vertebrate-bearing Bayn Shire formation in the Eastern Gobi Desert of Mongolia: usefulness of caliche for age determination. *Terra Nova*, **32**, 246–252.

Lehrmann, D., **Ramezani, J.**, **Bowring, S.**, **Martin, M.**, **Montgomery, P.**, **Enos, P.**, **Payne, J.**, **Orchard, M.**, **Hongmei, W.** and **Jiayong, W.** (2006) Timing of recovery from the end-Permian extinction: geochronologic and biostratigraphic constraints from south China. *Geology*, **34**, 1053.

Leng, M.J. and **Marshall, J.D.** (2004) Paleoclimate interpretation of stable isotope data from lake sediment archives. *Quat. Sci. Rev.*, **23**(7–8), 811–831.

Li, Q., **Parrish, R.R.**, **Horstwood, M.S.A.** and **McArthur, J.M.** (2014) U-Pb dating of cements in Mesozoic ammonites. *Chem. Geol.*, **376**, 7683.

Liivamägi, S., **Środoń, J.**, **Bojanowski, M.J.**, **Gerdes, A.**, **Stanek, J.J.**, **Williams, L.** and **Szczerba, M.** (2018) Paleosols on the Ediacaran basalts of the East European Craton: a unique record of paleoweathering with minimum diagenetic overprint. *Precambr. Res.*, **316**, 66–82.

Lougheed, B.C. and **Obrochta, S.P.** (2019) A rapid, deterministic age-depth modeling routine for geological sequences with inherent depth uncertainty. *Paleoceanogr. Paleoclimatol.*, **34**(1), 122–133.

Ludwig, K.R. (2012) User's manual for Isoplot Version 3.75–4.15: a Geochronological Toolkit for Microsoft Excel. *Berkeley Geochronological Center. Special Publication*, 5.

Machel, H.G. (1997) Recrystallization versus neomorphism, and the concept of 'significant recrystallization' in dolomite research. *Sediment. Geol.*, **113**(3–4), 161–168.

Machel, H.G. (2000) Application of cathodoluminescence to carbonate diagenesis. In: *Cathodoluminescence in Geosciences* (Eds Pagel, M., Barbin, V., Blanc, P. and Ohnenstetter, D.), pp. 127–160. Springer, Berlin, Heidelberg.

Mädel, F. (1984) Estratigrafıa del tramo inferior del pozo descubridor Palmar Largo x–1. *YPF Bol. Inf. Petrol.*, **1–2**, 109.

Mangenot, X., **Gasparrini, M.**, **Gerdes, A.**, **Bonifacie, M.** and **Rouchon, V.** (2018) An emerging thermochronometer for carbonate-bearing rocks: 147/(U-Pb). *Geology*, **46**, 1067–1070.

Marquillas, R.A. (1985) Estratigrafıa, sedimentologıa y paleoambientes de la Formacion Yacoraite (Cretacico Superior) en el tramo austral de la cuenca, norte argentino. Tesis Doctoral, Universidad Nacional de Salta, pp. 1–139.

Marquillas, R.A., **del Papa, C.**, **Sabino, I.** and **Heredia, J.** (2003) Prospección del límite K/T en la cuenca del Noroeste, Argentina. *Rev. Asoc. Geol. Argent.*, **58**(2), 271–274.

Marquillas, R.A., **Sabino, I.**, **Sial, N.A.**, **Del Papa, C.**, **Ferreira, V.** and **Matthews, S.** (2007) Carbon and oxygen isotopes of Maastrichtian-Danian shallow marine carbonates: Yacoraite Formation, northwestern Argentina. *J. S. Am. Earth Sci.*, **23**(4), 304–320.

Marquillas, R.A., **Salfity, J.A.**, **Matthews, S.J.**, **Matteini, M.** and **Dantas, E.** (2011) U-Pb zircon age of the Yacoraite Formation and its significance to the Cretaceous-Tertiary boundary in the Salta Basin, Argentina. In: *Cenezoic Geology of the Central Andes of Argentina* (Eds Salfity, J.A. and Marquillas, R.A.), pp. 227–246. SCS Publisher, Salta.

McManus, J., **Berelson, W.M.**, **Severmann, S.**, **Poulson, R.L.**, **Hammond, D.E.**, **Klinkhammer, G.P.** and **Holm, C.** (2006) Molybdenum and uranium geochemistry in continental margin sediments: paleoproxy potential. *Geochim. Cosmochim. Acta*, **70**, 4643–4662.

Meinhold, G., **Roberts, N.M.W.**, **Arslan, A.**, **Jensen, S.**, **Ebbestad, J.O.R.**, **Högström, A.E.S.**, **Høyberget, M.**, **Agić, H.**, **Palacios, T.** and **Taylor, W.L.** (2020) U-Pb dating of calcite in ancient carbonates for age estimates of syn- to post-depositional processes: a case study from the upper Ediacaran strata of Finnmark, Arctic Norway. *Geol. Mag.*, **157**, 1367–1372.

Miyajima, Y., **Saito, A.**, **Kagi, H.**, **Yokoyama, T.**, **Takahashi, Y.** and **Hirata, T.** (2021) Incorporation of U, Pb and rare earth elements in calcite through crystallisation from amorphous calcium carbonate: simple preparation of reference materials for microanalysis. *Geostand. Geoanal. Res.*, **45**(1), 189–205.

Montañez, I.P. and **Read, F.J.** (1992) Fluid-rock interaction history during stabilization of early dolomites, Upper Knox Group (Lower Ordovician) U.S. Appalachians. *J. Sediment. Petrol.*, **62**, 735–778.

Montano, D., **Gasparrini, M.**, **Gerdes, A.**, **Albert, R.** and **Della Porta, G.** (2021) In-situ U-Pb dating of Ries Crater lacustrine carbonates (Miocene, South-West Germany): implications for continental carbonate chronostratigraphy. *Earth Planet. Sci. Lett.*, **568**(1), 117011.

Moreno, J.A. (1970) Estratigrafía y paleogeografía del Cretácico superior en la cuenca del noroeste argentino, con especial mención de los Subgrupos Balbuena y Santa Bárbara. *Rev. Asoc. Geol. Argent.*, **24**, 9–44.

Moroni, A.M. (1982) Correlación palinológica en la Formaciones Olmedo y Yacoraite. Cuenca del Noroeste Argentino. 3o Congreso Geológico Chileno (Concepción), Actas, 340–349.

Moroni, A.M. (1984) *Congreso Argentino de Paleontología y Bioestratigrafía*, 3, 1982, pp. 129–139. Actas, Corrientes.

Mottram, C.M., **Kellett, D.A.**, **Barresi, T.**, **Zwingmann, H.**, **Friend, M.**, **Todd, A.** and **Percival, J.B.** (2020) Syncing fault rock clocks: direct comparison of U-Pb carbonate and K-Ar illite fault dating methods. *Geology*, **48**(12), 1179–1183.

Nicholson, S.L., **Pike, A.W.G.**, **Hosfield, R.**, **Roberts, N.**, **Sahy, D.**, **Woodhead, J.**, **Cheng, H.**, **Edwards, R.L.**, **Affolter, S.**, **Leuenberger, M.**, **Burns, S.J.**, **Matter, A.** and **Fleitmann, D.** (2020) Pluvial periods in Southern Arabia over the last 1.1 million-years. *Quat. Sci. Rev.*, **229**, 106112.

Nuriel, P., **Wotzlaw, J.**, **Ovtcharova, M.**, **Vaks, A.**, **Stremtan, C.**, **Šala, M.**, **Roberts, N.M.W.** and **Kylander-Clark, A.R.C.** (2021) The use of ASH-15 flowstone as a matrix-matched reference material for laser-ablation U − Pb geochronology of calcite. *Geochronology*, **3**, 35–47.

Omarini, R.H., **Salfity, J.A.**, **Linares, E.**, **Viramonte, J.G.** and **Gorustovich, S.A.** (1989) Petrologia geoquimica y edad de un filon lamproitico en el Subgrupo Pirgua (Alemania-Salta). *Rev. Inst. Geol. Miner.*, **7**, 89–99. (Universidad Nacional de Jujuy.)

Paquette, J.L., **Barbosa, J.**, **Rohais, S.**, **Cruz, S.**, **Goncalves, P.**, **Peucat, J.**, **Leal, A.**, **Santos-Pinto, M.** and **Martin, H.** (2015) The geological roots of South America: 4.1Ga and 3.7Ga zircon crystals discovered in N.E. Brazil and N.W. Argentina. *Precambrian Res.*, **271**, 49–55.

© 2022 The Authors. *Sedimentology* published by John Wiley & Sons Ltd on behalf of International Association of Sedimentologists, *Sedimentology*, **69**, 2507–2534

13653091, 2022, 6, Downloaded from https://onlinelibrary.wiley.com/doi/10.1111/sed.13000 by Ifp Energies Nouvelles, Wiley Online Library on [17/01/2023]. See the Terms and Conditions (https://onlinelibrary.wiley.com/terms-and-conditions) on Wiley Online Library for rules of use; OA articles are governed by the applicable Creative Commons License

Parrish, J.T., **Rasbury, E.T.**, **Chan, A.** and **Hasiotis, S.T.** (2019) Earliest Jurassic U-Pb ages from carbonate deposits in the Navajo Sandstone, southeastern Utah, USA. *Geology*, **47**(11), 1015–1019.

Pimentel, M., **Carmo, I.O.** and **Terra, G.J.S.** (2012) U-Pb age of tuffs from the Balbuena Group, Salta Basin, NW Argentina. In: VIII Simposio Sudamericano de Geologia Isotopica, Medellın. Resumos. Universidad Nacional de Colombia, Medellın.

Pupin, J.P. (1976) Signification des caractères morphologiques du zircon commun des roches en pétrologie. Base de la méthode typologique. Applications. (Thèse d'État), Université de Nice.

Quattrocchio, M. (2006) Palynology and palaeocommunities of the paleogene of Argentina. *Rev. Bras. Paleontol.*, **9**(1), 101–108.

Quattrocchio, M., **Volkheimer, W.**, **Marquillas, R.** and **Salfity, J.** (2005) Palynostratigraphy, palaeobiogeography and evolutionary significance of the Late Senonian and Early Palaeogene palynofloras of the Salta Group, northern Argentina. *Rev. Esp. Micropaleontol.*, **37**, 259–272.

Ramsey, C. and **Lee, S.** (2013) Recent and planned developments of the program OxCal. *Radiocarbon*, **55**(2), 720–730.

Rasbury, E.T. and **Cole, J.M.** (2009) Directly dating geologic events: U-Pb dating of carbonates. *Rev. Geophys.*, **47**, RG3001.

Rasbury, E.T., **Present, T.M.**, **Northrup, P.**, **Tappero, R.V.**, **Lanzirotti, A.**, **Cole, J.M.**, **Wooton, K.M.** and **Hatton, K.** (2021) Tools for uranium characterization in carbonate samples: case studies of natural U-Pb geochronology reference materials. *Geochronology*, **3**, 103–122.

Raskovsky, M.A. (1968) *Relevamiento geológico del sector sur delyacimiento Los Berthos [Seminario II]*. UniversidadNacional de Tucumán, Facultad de Ciencias Naturales, Salta, 41 pp.

Reyes, F.C. (1972) Correlaciones en el Cretácico de la cuenca andinade Bolivia, Perú y Chile: La Paz. *Rev. Téc. Yacim. Pet. Fisc. Boliv.*, **1**, 101–144.

Reyes, F.C. and **Salfity, J.A.** (1973) Consideraciones sobre la estratigrafía del Cretácico (Subgrupo Pirgua) del noroeste argentino. *Actas. 5th Congr. Geol. Argent.*, **3**, 355–385.

Ring, U. and **Gerdes, A.** (2016) Kinematics of the Alpenrhein-Bodensee grabensystem in the Central Alps: Oligocene/Miocene transtension due to formation of the Western Alps arc. *Tectonics*, **35**, 1367–1391. https://doi.org/10.1002/2015TC004085.

Roberts, N.M.W., **Drost, K.**, **Horstwood, M.S.A.**, **Condon, D.J.**, **Chew, D.**, **Drake, H.**, **Milodowski, A.E.**, **McLean, N.M.**, **Smye, A.J.**, **Walker, R.J.**, **Haslam, R.**, **Hodson, K.**, **Imber, J.**, **Beaudoin, N.** and **Lee, J.K.** (2020a) Laser ablation inductively coupled plasma mass spectrometry (LA-ICP-MS) U-Pb carbonate geochronology: strategies, progress, and limitations. *Geochronology*, **2**, 33–61.

Roberts, N.M.W., **Lee, J.K.**, **Holdsworth, R.E.**, **Jeans, C.**, **Farrant, A.F.** and **Haslam, R.** (2020b) Near-surface Palaeocene fluid flow, mineralisation and faulting at Flamborough Head, UK: new field observations and U-Pb calcite dating constraints. *Solid Earth*, **11**, 1931–1945.

Roberts, N.M.W., **Rasbury, T.**, **Parrish, R.R.**, **Smith, C.J.M.**, **Horstwood, M.S.A.** and **Condon, B.J.** (2017) A calcite reference material for LA-ICP-MS U-Pb geochronology. *Geochem. Geophys.*, **18**(7), 2807–2814.

Roberts, N.M.W. and **Walker, R.J.** (2016) U-Pb geochronology of calcite-mineralized faults: absolute timing of rift-related fault events on the northeast Atlantic margin. *Geology*, **44**, 531–534.

Roberts, N.M.W., **Žák, J.**, **Vacek, F.** and **Sláma, J.** (2021) No more blind dates with calcite: fluid-flow vs. fault-slip along the Očkov thrust, Prague Basin. *Geosci. Front.*, **12**(4), 101143.

Rohais, S., **Hamon, Y.**, **Deschamps, R.**, **Beaumont, V.**, **Gasparrini, M.**, **Pillot, D.** and **Romero-Sarmiento, M.** (2019) Patterns of organic carbon enrichment in a lacustrine system across the K-T boundary: insight from a multi-proxy analysis of the Yacoraite Formation, Salta rift basin, Argentina. *Int. J. Coal Geol.*, **210**, 103208.

Rossignol, C., **Hallot, E.**, **Bourquin, S.**, **Poujol, M.**, **Jolivet, M.**, **Pellenard, P.**, **Ducassou, C.**, **Nalpas, T.**, **Heilbronn, G.**, **Yu, J.** and **Dabard, M.** (2019) Using volcaniclastic rocks to constrain sedimentation ages: to what extent are volcanism and sedimentation synchronous? *Sed. Geol.*, **381**, 46–64.

Sadler, P.M. (1981) Sediment accumulation rates and the completeness of stratigraphic sections. *J. Geol.*, **89**, 569–584.

Salfity, J.A. (1979) Paleogeologıa de la cuenca del Grupo Salta (Cretacico-Eogenico) del norte de Argentina. *Actas. 7th Congr. Geol. Argent.*, **1**, 505–515.

Salfity, J.A. and **Marquillas, R.A.** (1994) Tectonic and sedimentary evolution of the Cretaceous-Eocene Salta Group Basin, Argentina. In: *Cretaceous Tectonics of the Andes. Earth Evolution Sciences* (Eds Salfity, J.A.). Vieweg+Teubner Verlag, Wiesbaden. https://doi.org/10.1007/978-3-322-85472-8_6

Saller, A., **Rushton, S.**, **Buambua, L.**, **Inman, K.**, **McNeil, R.** and **Dickson, J.A.D.T.** (2016) Presalt stratigraphy and depositional systems in the Kwanza Basin, offshore Angola. *AAPG Bull.*, **100**(7), 1135–1164.

Santos, M.M., **Lana, C.**, **Scholz, R.**, **Buick, I.**, **Schmitz, M.D.**, **Kamo, S.L.**, **Gerdes, A.**, **Corfu, F.**, **Tapster, S.**, **Lancaster, P.**, **Storey, C.D.**, **Basei, M.A.S.**, **Tohver, E.**, **Alkmim, A.**, **Nalini, H.**, **Krambrock, K.**, **Fantini, C.** and **Wiedenbeck, M.** (2017) A new appraisal of Sri Lankan BB zircon as a reference material for LA-ICP-MS U-Pb geochronology and Lu-Hf isotope tracing. *Geostand. Geoanal. Res.*, **41**(3), 335–358.

Scardia, G., **Parenti, F.**, **Miggins, D.P.**, **Gerdes, A.**, **Araujo, A.G.** and **Neves, W.A.** (2019) Chronologic constraints on hominin dispersal outside Africa since 2.48 Ma from the Zarqa Valley, Jordan. *Quat. Sci. Rev.*, **219**, 1–19.

Schoene, B., **Samperton, K.M.**, **Eddy, M.P.**, **Keller, G.**, **Adatte, T.**, **Bowring, S.A.**, **Khadri, S.F.R.** and **Gertsch, B.** (2015) U-Pb geochronology of the Deccan Traps and relation to the end Cretaceous mass extinction. *Science*, **347**(6218), 182–184.

Schumer, R. and **Jerolmack, D.J.** (2009) Real and apparent changes in sediment deposition rates through time. *J. Geophys. Res.*, **114**, F00A06. https://doi.org/10.1029/2009JF001266

Sial, A., **Ferreira, V.**, **Toselli, A.**, **Parada, M.**, **Aceñolaza, F.**, **Pimentel, M.** and **Alonso, R.** (2001) Carbon and oxygen isotope compositions of some upper cretaceous-paleocene sequences in Argentina and Chile. *Int. Geol. Rev.*, **43**, 892–909.

Sial, A.N., **Lacerda, L.D.**, **Ferreira, V.P.**, **Frei, R.**, **Marquillas, R.A.**, **Barbosa, J.A.**, **Gaucher, C.**, **Windmöller, C.C.** and **Pereira, N.S.** (2013) Mercury as a proxy for volcanic activity during extreme environmental turnover: the Cretaceous-Paleogene transition. *Palaeogeogr. Palaeoclimatol. Palaeoecol.*, **387**, 153–164.

© 2022 The Authors. *Sedimentology* published by John Wiley & Sons Ltd on behalf of International Association of Sedimentologists, *Sedimentology*, **69**, 2507–2534

13653091, 2022, 6, Downloaded from https://onlinelibrary.wiley.com/doi/10.1111/sed.13000 by Ifp Energies Nouvelles, Wiley Online Library on [17/01/2023]. See the Terms and Conditions (https://onlinelibrary.wiley.com/terms-and-conditions) on Wiley Online Library for rules of use; OA articles are governed by the applicable Creative Commons License

Simone, L. (1980) Ooids: a review. *Earth Sci. Rev.*, **16**, 319–355.

Sláma, J., **Košler, J.**, **Condon, D.J.**, **Crowley, J.L.**, **Gerdes, A.**, **Hanchar, J.M.**, **Horstwood, M.S.A.**, **Morris, G.A.**, **Nasdala, L.**, **Norberg, N.**, **Schaltegger, U.**, **Schoene, B.**, **Tubrett, M.N.** and **Whitehouse, M.J.** (2008) Plešovice zircon — a new natural reference material for U-Pb and Hf isotopic microanalysis. *Chem. Geol.*, **249**(1–2), 1–35.

Smith, P.E. and **Farquhar, R.M.** (1989) Direct dating of Phanerozoic sediments by the ^{238}U single bond ^{206}Pb method. *Nature*, **341**, 518–521.

Środoń, J., **Gerdes, A.**, **Kramers, J.** and **Bojanowski, M.J.** (2022) Age constraints of the Sturtian glaciation on western Baltica based on U-Pb and Ar-Ar dating of the Lapichi Svita. *Precambr. Res.*, **371**, 106595.

Starck, D. (2011) *Cuenca Cretácica-Paleógena del Noroeste Argentino. VIII Congreso de Exploración y Desarrollo de Hidrocarburos.* Simposio de Cuencas Argentinas: visión actual, Mar del Plata, pp. 407–453.

Suarez-Gonzalez, P., **Benito, M.I.**, **Quijada, I.E.**, **Mas, R.** and **Campos-Soto, S.** (2019) 'Trapping and binding': a review of the factors controlling the development of fossil agglutinated microbialites and their distribution in space and time. *Earth Sci. Rev.*, **194**, 182–215.

Swart, P.K. (2015) The geochemistry of carbonate diagenesis: the past, present and future. *Sedimentology*, **62**, 1233–1304.

Talbot, M.R. (1990) A review of the palaeohydrological interpretation of carbon and oxygen isotopic ratios in primary lacustrine carbonates. *Isot. Geosci.*, **8**(4), 261–279.

Thompson, D.L., **Stilwell, J.D.** and **Hall, M.** (2015) Lacustrine carbonate reservoirs from Early Cretaceous rift lakes of Western Gondwana: pre-salt coquinas of Brazil and west Africa. *Gondwana Res.*, **28**(1), 26–51.

Tribovillard, N., **Algeo, T.J.**, **Lyons, T.** and **Riboulleau, A.** (2006) Trace metals as paleoredox and paleoproductivity proxies; an update. *Chem. Geol.*, **232**(1–2), 12–32.

Valais, S. and **Cónsole-Gonella, C.** (2019) An updated review of the avian footprint record from the yacoraite formation (Maastrichtian-Danian), Northwestern Argentina. *Ichnos*, **26**, 224–241.

Van Wagoner, J.C., **Posamentier, H.W.**, **Mitchum, R.M.**, **Vail, P.R.**, **Sarg, J.F.**, **Loutit, T.S.** and **Hardenbol, J.** (1988) An overview of the fundamentals of sequence stratigraphy and key definitions. In: *Sea-level Changes: An Integrated Approach* (Eds Wilgus, C.K., Hastings, B.S., Kendall, C.G.S.C., Posamentier, H.W., Ross, C.A. and Van Wagoner, J.C.), *Soc. Sediment. Geol. Spec. Publ.*, **42**, 39–45.

Veizer, J. (1983) Chemical diagenesis of carbonates: theory and application of trace element technique. *Stable Isotopes Sediment. Geol.*, **10**, 3.1–3.100.

Veizer, J., **Ala, D.**, **Azmy, K.**, **Bruckschen, P.**, **Buhl, D.**, **Bruhn, F.**, **Carden, G.A.F.**, **Diener, A.**, **Ebneth, S.**, **Godderis, Y.**, **Jasper, T.**, **Korte, C.**, **Pawellek, F.**, **Podlaha, O.G.** and **Strauss, H.** (1999) $^{87}Sr/^{86}Sr$, $\delta^{13}C$ and $\delta^{18}O$ evolution of Phanerozoic seawater. *Chem. Geol.*, **161**(13), 59–88.

Volkheimer, W., **Novara, M.**, **Narváez, P.** and **Marquillas, R.** (2006) Palynology and paleoenvironmental significance of the Tunal Formation (Danian) at its type locality, El Chorro creek (Salta, Argentina). *AMEGHINIANA (Rev. Asoc. Paleontol. Argent.)*, **43**(3), 567–584.

Wainman, C.C., **McCabe, P.J.** and **Crowley, J.L.** (2018) Solving a tuff problem: defining a chronostratigraphic framework for Middle to Upper Jurassic non marine strata in eastern Australia using uranium–lead chemical abrasion–thermal ionization mass spectrometry zircon dates. *AAPG Bull.*, **102**(6), 1141–1168.

Walter, B.F., **Gerdes, A.**, **Kleinhanns, I.C.**, **Dunkl, I.**, **Eynatten, H.V.**, **Kreissl, S.** and **Markl, G.** (2018) The connection between hydrothermal fluids, mineralization, tectonics and magmatism in a continental rift setting: fluorite Sm-Nd and hematite and carbonates U-Pb geochronology from the Rhinegraben in SW Germany. *Geochim. Cosmochim. Acta*, **240**, 11–42.

Watson, E., **Swindles, G.**, **Lawson, I.**, **Savov, I.** and **Wastegård, S.** (2017) The presence of Holocene cryptotephra in Wales and southern England. *J. Quat. Sci.*, **32**, 493–500.

Wiedenbeck, M., **Allé, P.**, **Corfu, F.**, **Griffin, W.L.**, **Meier, M.**, **Oberli, F.**, **Quadt, A.V.**, **Roddick, J.C.** and **Spiegel, W.** (1995) Three natural zircons standards for U-Th-Pb, Lu-Hf, Trace element and REE analyses. *Geostand. Newslett.*, **19**(1), 1–23.

Williams, I.S. and **Claesson, S.** (1987) Isotopic evidence for the Precambrian provenance and Caledonian metamorphism of high grade paragneisses from the Seve Nappes, Scandinavian Caledonides. II: Ion microprobe zircon U-Th-Pb. *Contrib. Mineral. Petrol.*, **97**, 205–217.

Woodhead, J. and **Petrus, J.A.** (2019) Exploring the advantages and limitations of in situ U-Pb carbonate geochronology using speleothems. *Geochronology*, **1**(1), 69–84.

Wotzlaw, J., **Hüsing, S.**, **Hilgen, F.** and **Schaltegger, U.** (2014) High-precision zircon U-Pb geochronology of astronomically dated volcanic ash beds from the Mediterranean Miocene. *Earth Planet. Sci. Lett.*, **407**, 19–34.

Yang, P., **Liu, K.**, **Li, Z.**, **Rankenburg, K.**, **McInnes, B.I.A.**, **Liu, J.** and **Evans, N.J.** (2022) Direct dating Paleo-fluid flow events in sedimentary basins. *Chem. Geol.*, **588**, 120642.

Manuscript received 19 July 2021; revision accepted 11 April 2022

Supporting Information

Additional information may be found in the online version of this article:

Appendix S1. Settings of the Laser and of the ICP-MS instrument for zircon and carbonate dating sessions.

Appendix S2. $^{238}U/^{206}Pb$ versus $^{207}Pb/^{206}Pb$ Tera-Wasserburg Concordia diagrams and corresponding absolute ages for the carbonate samples successfully dated (n = 19).

© 2022 The Authors. *Sedimentology* published by John Wiley & Sons Ltd on behalf of International Association of Sedimentologists, *Sedimentology*, **69**, 2507–2534

13653091, 2022, 6, Downloaded from https://onlinelibrary.wiley.com/doi/10.1111/sed.13000 by Ifp Energies Nouvelles, Wiley Online Library on [17/01/2023]. See the Terms and Conditions (https://onlinelibrary.wiley.com/terms-and-conditions) on Wiley Online Library for rules of use; OA articles are governed by the applicable Creative Commons License